Article

Cell Reports

Single-Cell Transcriptomics Identifies the Adaptation of Scart1$^+$ Vγ6$^+$ T Cells to Skin Residency as Activated Effector Cells

Graphical Abstract

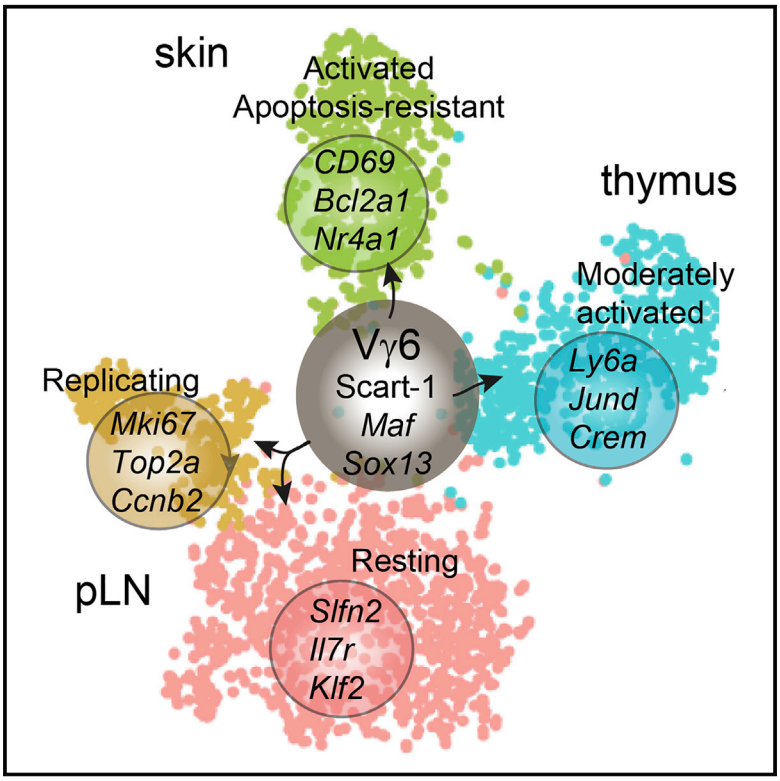

Highlights

- Single-cell RNA-seq reveals differential tissue-specific adaptation of Vγ6$^+$ T cells
- Skin Vγ6$^+$ T cells show an activated IL-17- and amphiregulin-producing effector phenotype
- Expression of Bcl2a1 family proteins protect activated skin Vγ6$^+$ T cells from apoptosis
- Skin Vγ6$^+$ and Vγ4$^+$ T cells can be distinguished by Scart1 versus Scart2 expression

Authors

Likai Tan, Inga Sandrock, Ivan Odak, ..., Christian Krebs, Immo Prinz, Sarina Ravens

Correspondence

prinz.immo@mh-hannover.de (I.P.), ravens.sarina@mh-hannover.de (S.R.)

In Brief

Tan et al. apply single-cell transcriptome analysis of tissue-resident Vγ6$^+$ T cells and identify molecular determinants that mediate the functional adaptation and longevity of Scart1$^+$ Vγ6$^+$ T cells within tissues.

Tan et al., 2019, Cell Reports *27*, 3657–3671
June 18, 2019
https://doi.org/10.1016/j.celrep.2019.05.064

CellPress

Cell Reports
Article

Single-Cell Transcriptomics Identifies the Adaptation of Scart1$^+$ Vγ6$^+$ T Cells to Skin Residency as Activated Effector Cells

Likai Tan,[1,10] Inga Sandrock,[1,10] Ivan Odak,[1] Yuval Aizenbud,[2] Anneke Wilharm,[1] Joana Barros-Martins,[1] Yaara Tabib,[2] Alina Borchers,[3] Tiago Amado,[4] Lahiru Gangoda,[5,6] Marco J. Herold,[5,6] Marc Schmidt-Supprian,[7] Jan Kisielow,[8] Bruno Silva-Santos,[4] Christian Koenecke,[1,9] Avi-Hai Hovav,[2] Christian Krebs,[3] Immo Prinz,[1,11,*] and Sarina Ravens[1,11,12,*]

[1]Institute of Immunology, Hannover Medical School, 30625 Hannover, Germany
[2]Institute of Dental Sciences, Faculty of Dental Medicine, Hebrew University, Jerusalem 91120, Israel
[3]Department of Medicine, University Medical Center Hamburg-Eppendorf, 20251 Hamburg, Germany
[4]Instituto de Medicina Molecular, Faculdade de Medicina, Universidade de Lisboa, Lisbon, Portugal
[5]Walter and Eliza Hall Institute of Medical Research, Parkville, VIC 3052, Australia
[6]Department of Medical Biology, University of Melbourne, Parkville, VIC 3052, Australia
[7]Institute of Experimental Hematology, TranslaTUM, Klinikum rechts der Isar der Technischen Universität München, 81675 Munich, Germany
[8]Institute of Molecular Health Science, ETH Zuerich, 8093 Zuerich, Switzerland
[9]Department of Hematology, Hemostasis, Oncology and Stem Cell Transplantation, Hannover Medical School, 30625 Hannover, Germany
[10]These authors contributed equally
[11]Senior author
[12]Lead Contact
*Correspondence: prinz.immo@mh-hannover.de (I.P.), ravens.sarina@mh-hannover.de (S.R.)
https://doi.org/10.1016/j.celrep.2019.05.064

SUMMARY

IL-17-producing $\gamma\delta$ T cells express oligoclonal Vγ4$^+$ and Vγ6$^+$ TCRs, mainly develop in the prenatal thymus, and later persist as long-lived self-renewing cells in all kinds of tissues. However, their exchange between tissues and the mechanisms of their tissue-specific adaptation remain poorly understood. Here, single-cell RNA-seq profiling identifies IL-17-producing Vγ6$^+$ T cells as a highly homogeneous Scart1$^+$ population in contrast to their Scart2$^+$ IL-17-producing Vγ4$^+$ T cell counterparts. Parabiosis demonstrates that Vγ6$^+$ T cells are fairly tissue resident in the thymus, peripheral lymph nodes, and skin. There, Scart1$^+$ Vγ6$^+$ T cells display tissue-specific gene expression signatures in the skin, characterized by steady-state production of the cytokines IL-17A and amphiregulin as well as by high expression of the anti-apoptotic Bcl2a1 protein family. Together, this study demonstrates how Scart1$^+$ Vγ6$^+$ T cells undergo tissue-specific functional adaptation to persist as effector cells in their skin habitat.

INTRODUCTION

$\gamma\delta$ T cells constitute a major T lymphocyte population in mucosal tissues and the skin and a minor T cell fraction within lymphoid organs. $\gamma\delta$ T cells producing the pro-inflammatory cytokines interleukin-17A (IL-17A) and IL-17F ($\gamma\delta$T17) were ascribed pleiotropic functions: they can mediate local immune responses against fungal or bacterial infections (Hamada et al., 2008; Lockhart et al., 2006; Murphy et al., 2014; Sheridan et al., 2013; Shibata et al., 2007; Sumaria et al., 2011), contribute to tissue homeostasis during anti-viral responses (Guo et al., 2018) and periodontitis (Krishnan et al., 2018), and regulate body thermogenesis (Kohlgruber et al., 2018). Moreover, $\gamma\delta$T17 cells are involved in the pathology of local inflammatory immune diseases, such as arthritis (Reinhardt et al., 2016; Roark et al., 2007), experimental autoimmune encephalomyelitis (Petermann et al., 2010), or psoriasis (Cai et al., 2011; Hartwig et al., 2015; Pantelyushin et al., 2012; Sandrock et al., 2018) as well as cancer (Silva-Santos et al., 2015). The T cell receptors (TCRs) of $\gamma\delta$T17 cells show little or no junctional diversity, and the TCR repertoire is enriched for oligoclonal Vγ6$^+$ or Vγ4$^+$ γ-chains (Heilig and Tonegawa nomenclature; Hayday et al., 1985). The TCR repertoire of Vγ6$^+$ $\gamma\delta$T17 cells is dominated by one major invariant Vγ6Vδ1$^+$ clone lacking additional N-nucleotide insertions (Itohara et al., 1990; Wei et al., 2015) and few semi-invariant Vγ6Vδ1$^+$ clones (Fujikado et al., 2016; Sandrock et al., 2018), whereas Vγ4$^+$ $\gamma\delta$T17 cells have an oligoclonal TCR repertoire with multiple (semi)-invariant TCRs (Kashani et al., 2015; Wei et al., 2015). The generation of highly invariant TCRs during murine intrathymic development is very similar to human-fetal-derived Vγ9$^+$ $\gamma\delta$ T cells, which are proposed to circulate as a long-lived population in the peripheral blood after birth (Dimova et al., 2015; Vermijlen and Prinz, 2014). Comparably, the development of innate $\gamma\delta$T17 cells is restricted to the embryonic thymus where they acquire the capacity to produce IL-17 prior to becoming pre-activated CD27$^-$, CD44^{high} $\gamma\delta$T17 cells (Haas et al., 2012; Ribot et al., 2009; Shibata et al., 2008; Spidale et al., 2018). This IL-17 production fate is coordinated by expression of various transcription factors (e.g., Sox-proteins, Notch, Heb, and PLZF) during early intra-thymic development (Gray et al., 2013; In et al., 2017; Lu et al., 2015; Mair et al., 2015; Malhotra

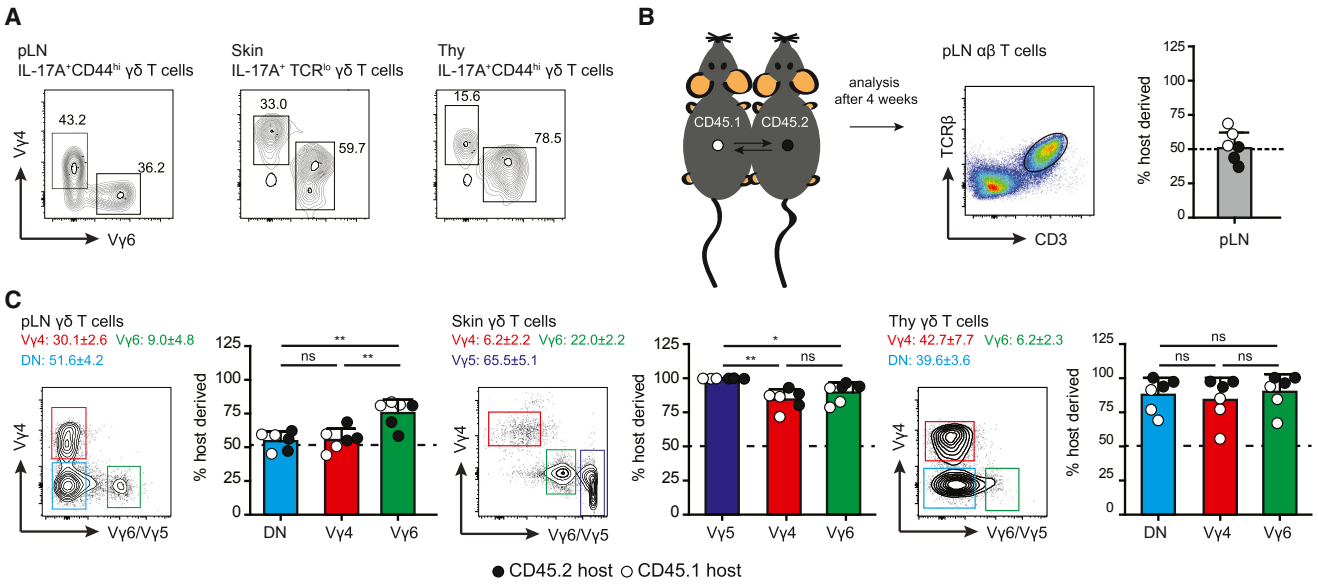

Figure 1. IL-17-Producing Vγ6$^+$ T Cells Are Mainly Tissue Resident

(A) Frequencies of Vγ4$^+$ and Vγ6$^+$ γδ T cells among IL-17A-producing CD44^{high} γδ T cells in the indicated organs. Cells were measured after overnight IL-23 stimulation.

(B and C) CD45.1$^+$ and CD45.2$^+$ congenic mice were analyzed after 4 weeks of parabiosis by flow cytometry.

(B) Representative dot plot of pLN αβ T cells. Scatterplot shows frequency of host-derived αβ T cells in pLN.

(C) Contour plots show gating and mean frequencies ± SD of Vγ4$^+$, Vγ6/5$^+$, and double-negative (DN) γδ T cells. Scatterplots show proportions of host-derived γδ T cells among indicated subsets. Pooled data of three pairs of parabiotic mice, mean + SD, one-way ANOVA with Bonferroni post-tests (not significant [ns] $p > 0.05$, *$p < 0.05$, **$p < 0.01$, ***$p < 0.001$).

et al., 2013; Narayan et al., 2012; Powolny-Budnicka et al., 2011; Shibata et al., 2011; Spidale et al., 2018). Of note, the defined transcription factor expression programs intrinsically prime γδ T cells to become IL-17 producers prior to and independent of TCR signaling (Haas et al., 2012; Spidale et al., 2018). The fact that the inflammatory cytokine IL-23 induces immediate production of IL-17 on peripheral Vγ6$^+$ or Vγ4$^+$ T cells further reflects their innate capability to directly enhance inflammatory responses (Petermann et al., 2010; Sutton et al., 2009). However, other studies suggested that TCR stimulation or IL-23 can drive the peripheral differentiation of naive Vγ4$^+$ γδ T cells into IL-17 producers (Muschaweckh et al., 2017; Papotto et al., 2017; Zeng et al., 2012). Thus, the view of strictly innate, fetal-derived γδT17 cells might apply only to Vγ6$^+$ and a fraction of invariant fetal-thymus-derived Vγ4$^+$ γδT17 cells.

It appears that all Vγ6$^+$ and a subset of Vγ4$^+$ γδT17 cells are primed during early life to subsequently home to specific anatomic locations, to undergo local homeostatic expansion, and to functionally adapt to their respective tissue niches. To this end, several chemokine receptors, such as CCR2, CCR6 and CXCR6, are important for trafficking and recruitment of activated Vγ6$^+$ and Vγ4$^+$ γδT17 cells to tissues (Cai et al., 2014; Gray et al., 2011; McKenzie et al., 2017; Ramírez-Valle et al., 2015; Zhang et al., 2016). Expression of scavenger receptors (Scart1 and Scart2) may convey specific homing capabilities to γδT17 cells (Fink et al., 2010; Kisielow et al., 2008; Muzaki et al., 2017). However, in contrast to dendritic epidermal T cells (DETCs), the prototype of tissue-resident cells locating solely to the epidermis (Carding and Egan, 2002), γδT17 cells might under certain circumstances be able to re-circulate between tissues (Audemard-Verger et al., 2017; Romagnoli et al., 2016; Zhang et al., 2016). Although specialized γδT17 cells sharing the same invariant Vγ6$^+$ TCR have recently been identified within diverse peripheral tissues, such as skin, enthesis, or gingiva (Cai et al., 2011; Gray et al., 2011; Kohlgruber et al., 2018; Reinhardt et al., 2016; Sumaria et al., 2011; Wilharm et al., 2019), there is little information about their tissue residency and the gene expression programs that direct their functional adaptation and terminal differentiation within a given anatomic location.

Here, we addressed the tissue residency of Vγ4$^+$ and Vγ6$^+$ T cells by using adult parabiotic mice and could show that especially Vγ6$^+$ T cells are mainly but not exclusively tissue resident. Next, we used single-cell RNA sequencing (RNA-seq) technology to characterize transcriptional programs governing the tissue-specific adaptation of Vγ6$^+$ T cells isolated from thymus, peripheral lymph node,s and skin and compared them to their Vγ4$^+$ T cell counterparts in skin.

RESULTS

Vγ6$^+$ T Cells Are Mainly Tissue Resident

γδ T cells are a major source for IL-17A and IL-17F in lymphoid and non-lymphoid tissues (Papotto et al., 2018). Flow cytometric analyses revealed that γδ T cells with an IL-17-producing phenotype (CD27$^-$CD44^{high}) expressed mainly Vγ6$^+$ or Vγ4$^+$ TCR γ-chains (Figure 1A). To study the tissue residency of Vγ4$^+$ and

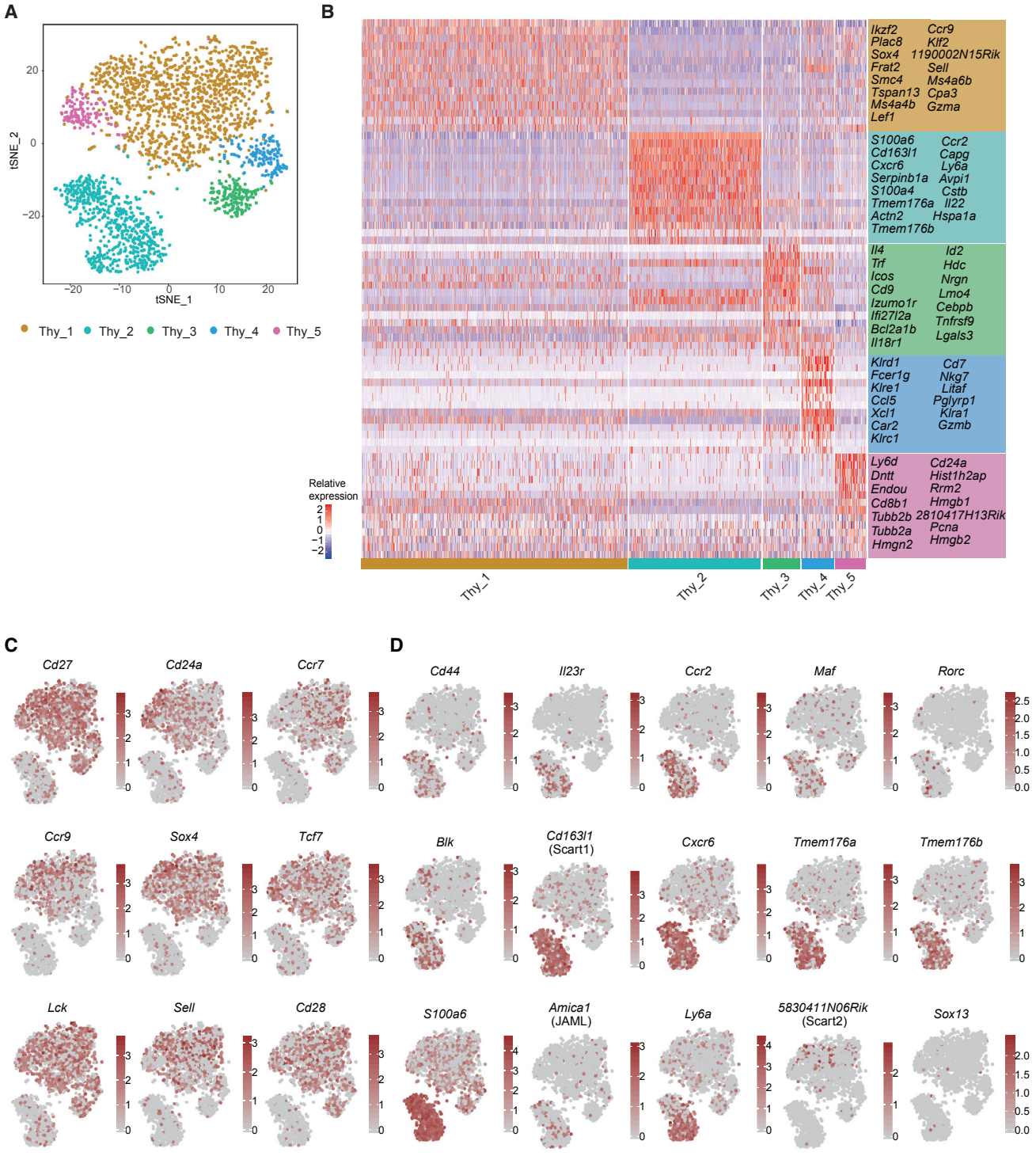

Figure 2. Single-Cell RNA-Seq Identifies γδT17 Cells in Thymus

Single-cell transcriptome libraries were generated of FACS-sorted $V\gamma6^+$ thymocytes.

(A) tSNE visualization of the γδ T cells in thymus after non-linear dimensional reduction analysis. Cells are colored by clusters from un-supervised clustering. Each point represents a single cell.

(legend continued on next page)

Vγ6$^+$ T cells, we generated parabiotic mice with the congenic markers CD45.1 and CD45.2. αβ T cells circulated readily in secondary lymphoid organs, and after 4 weeks of parabiosis, we observed complete chimerism for αβ T cells, as indicated by the equal distribution of CD45.1 and CD45.2 cells within the hosts (Figure 1B). Similarly, in peripheral lymph nodes (pLNs) Vγ4/Vγ6 double-negative and Vγ4$^+$ γδ T cells were equally host- and donor-derived and, thus, freely exchanging (Figure 1C, left). On the other hand, skin DECTs (Vγ5$^+$) were entirely of host origin (99.57% ± 0.15%), confirming their non-circulating phenotype (Figure 1C, middle). In contrast to DETCs, Vγ6$^+$ T cells were partially, but not exclusively, tissue resident in pLN (75.35% ± 9.97%), thymus (90.10% ± 12.86%), and skin (89.55% ± 7.23%). Additionally, thymus (84.10% ± 16.17%) and skin (84.42% ± 7.48%) Vγ4$^+$ T cells mainly resided in the tissue, whereas pLN Vγ4$^+$ T cells (55.52% ± 8.26%) displayed a circulating phenotype (Figure 1C). Altogether, these data support the idea that γδT17 cells can be selectively trapped in lymph nodes and that, in the steady-state, Vγ6$^+$ γδT17 cells are principally, but not exclusively, tissue resident. Therefore, these data suggest that Vγ6$^+$ T cells locally adapt as resident cells to specific sites of the body but possibly retain the capability to circulate between tissues.

Single-Cell Transcriptome Analysis Identifies Tissue-Resident Vγ6$^+$ γδT17 Cells within Thymus

We next applied droplet-based single-cell transcriptomics to better understand gene expression programs associated with thymus residency of γδT17 cell populations. For this purpose, thymus Vγ6$^+$ γδ T cells were isolated by flow cytometric sorting for single-cell RNA-seq analysis, as described in the methods section (Figures S1A and S1B; STAR Methods). We obtained single-cell transcriptomes of 2,414 γδ thymocytes. Principal component analysis for dimensional reduction and unsupervised clustering were performed, and t-Distributed Stochastic Neighbor Embedding (t-SNE) was adopted for data visualization. We identified five separate thymus clusters and especially the cluster 2 (Thy_2) clearly detached from the other four clusters (Figure 2A). All five clusters can be defined by differentially expressed genes (DEGs) (Figure 2B). Among the DEGs distinguishing the respective cell clusters, transcriptional regulators, transmembrane proteins, and cytokine and chemokine receptors were identified (Figure 2B). It is well established that adult thymi harbor only mature Vγ6$^+$ γδT17 cells being CD24$^-$ CD27$^-$CD44^{high} and that immature or interferon (IFN)-γ-producing γδ T cells can be defined by CD27 surface marker expression (Haas et al., 2009; Ribot et al., 2009) (Figure S1C). Here, we focused on the tissue-specific adaptation of mature Vγ6$^+$ γδT17 cells. However, due to difficulties with cell purity of fluorescence-activated cell sorting (FACS)-sorted Vγ6$^+$ thymocytes (Figure S1A), we first examined the expression of genes related to γδ T cell development and naive or IL-17-producing phenotypes in all five thymus clusters. With the exception of cluster 2, all clusters expressed selected surface markers, chemokine receptors, and transcription factors characteristic for immature γδ thymocytes (e.g., *Cd24a*, *Cd27*, *Ccr9*, *Ccr7*, and *Sox4*) (Malhotra et al., 2013; Reinhardt et al., 2014; Ribot et al., 2009) (Figure 2C). Moreover, all *Cd27*$^+$ thymocytes displayed high *Lck* gene expression, which encodes a central kinase involved in TCR signaling (Figure 2C). Importantly, we identified mature γδT17 cells within cluster 2 by expression of common marker genes of IL-17 producing T cells, such as *Cd44*, *Ccr2*, *Cxcr6*, *Il23r*, *Blk*, and *Maf*, whereas *Sox13* and *Rorc* mRNAs were rarely detectable (Bauquet et al., 2009; Ciofani et al., 2012; McKenzie et al., 2017; Petermann et al., 2010; Ribot et al., 2009; Spidale et al., 2018; Zuberbuehler et al., 2019) (Figure 2D).

We further noted that Scart2 (*5830411N06Rik*), which is highly expressed in IL-17-pre-committed Vγ4$^+$ thymocytes (Spidale et al., 2018), was rarely found in Vγ6$^+$ thymocytes, whereas *Cd163l1* (Scart1) was readily detected in the Vγ6$^+$ γδT17 cell population (cluster 2) (Figure 2D). Similar to *Cd163l1*, *Ly6a*, *Tmem176a/b*, and *S100a* mRNAs were exclusively present in cluster 2 and contribute to the unique biology of mature CD44$^+$ Vγ6$^+$ γδT17 cells (Figure 2D; Figure S1D). In addition, *Amica1* (JAML), which has been described as a co-stimulatory receptor of skin DETCs (Witherden et al., 2010), was detected in *Cd27*$^-$*Cd44*$^+$Vγ6$^+$ γδ T cells (cluster 2) (Figure 2D; Figure S1D).

Next, we generated additional single-cell transcriptome libraries of highly pure Vγ6$^+$ T cells isolated from pLN and skin (Figure S2) and analyzed those together with the γδ thymocyte dataset by keeping organ and library identity. Non-linear dimensional reduction analysis of the aggregated expression matrices identified two pLNs, one skin and five thymus clusters, which clearly segregated according to the respective tissues of origin (Figure S3A). To further confirm the γδT17 phenotype of Vγ6$^+$ γδ T cells within the respective clusters, cells were scored against gene signatures of immature, naïve, or IL-17-committed T cells (Figure S3B). In line with these analyses, we considered cells of thymus cluster 2 (*Cd24*$^-$, *Cd27*$^-$, and *Cd44*$^+$) as the thymus-resident, mature Vγ6$^+$ γδT17 cell population. For further downstream analysis, only single-cell transcriptomes of Vγ6$^+$ γδ T cells with a γδT17 phenotype were included hereafter (Figure S3C). In addition, this first experiment was fully validated by a second dataset retrieving highly similar results (Figure S4).

In summary, coincident single-cell transcriptome analysis of γδ thymocytes being either CD27$^+$CD44^{low} or CD27$^-$CD44^{high} allowed us to compare immature, naive polyclonal γδ T cells versus mature Vγ6$^+$ γδT17 cells, respectively. Hence, we identified Vγ6$^+$ γδT17 cells by previously described common (e.g., *Cd44*, *Ccr2*, *IL23r*, and *Blk*) and potentially new and specific (e.g., *Amica1*, *Cd163l1* (Scart1), *Tmem176a*, and *S100a6*) lineage-defining signature genes.

(B) Heatmap shows the top 10 upregulated DEGs of the respective clusters 1–5, identified in in the tSNE plot. Each column is the expression profile of a single cell. Gene expression values are scaled by Log2 fold change (logFC). DEGs are defined with a detection rate at least one cluster (min-pct) of ≥10%, logFC of ≥0.5, and adjusted p ≤ 0.01 (by Wilcoxon rank-sum test).

(C and D) Gene expression features in tSNE map of DEGs (C) in immature and naive γδ T cells clusters and (D) mature γδ T cells with an IL-17-producing phenotype. Scale in log expression.

See also Figures S1, S2, S3, and S4.

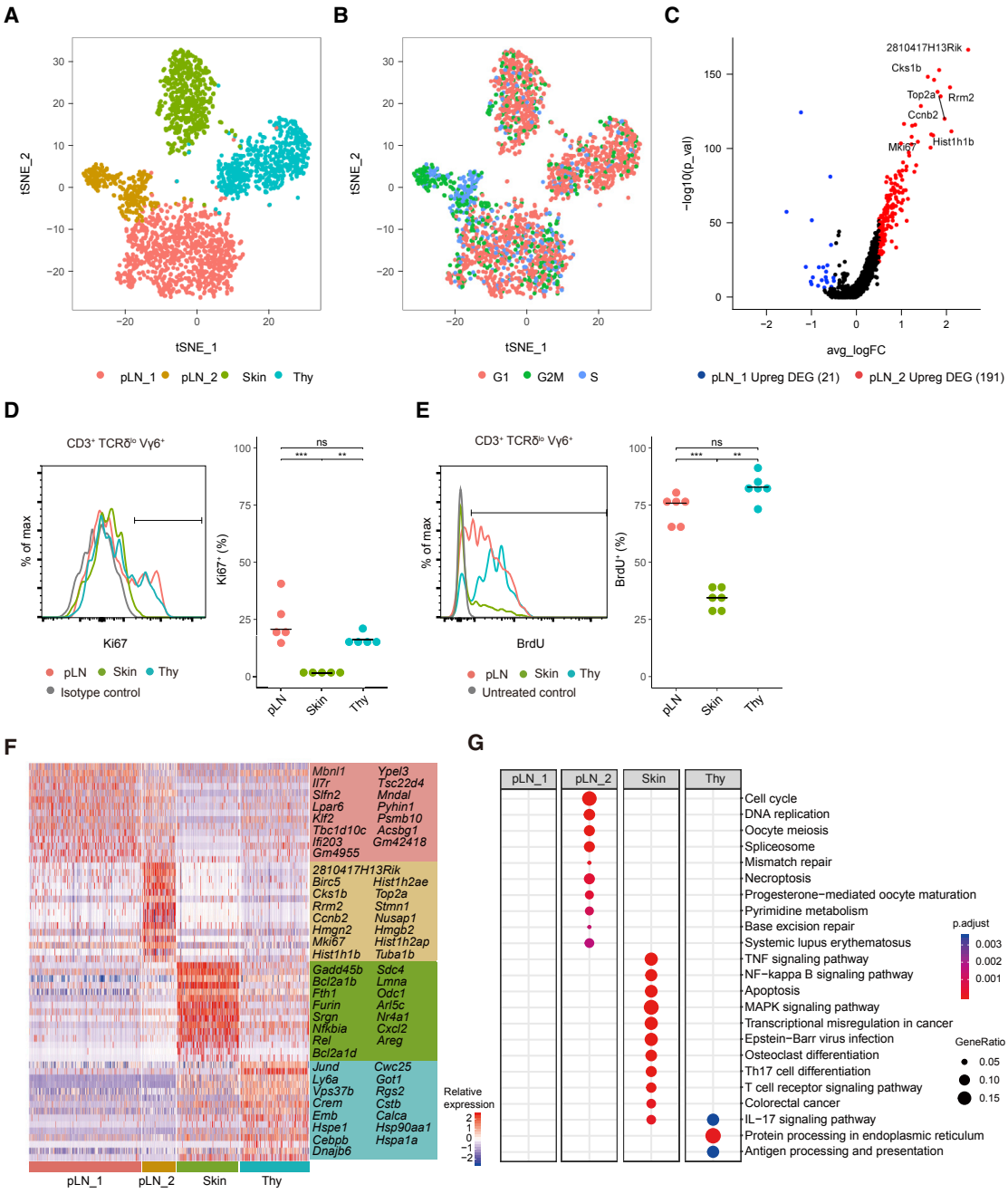

Figure 3. Vγ6⁺ T Cells Form Homogeneous but Distinct Subsets within Tissues

Integrated single-cell RNA-seq analysis of Vγ6⁺ T cells from pLN, ear skin, and thymus.

(A) The cleaned dataset from Figure S2D was analyzed further. The global mRNA expression profile of each cell is subjected to non-linear dimensional reduction analysis and un-supervised clustering and visualized by tSNE map. Cells are colored according to their cluster, and each point represents a single cell.

(B) Module scores calculated from the expression of cell-cycle-related genes assigned each cell to the cell cycle phase are shown on the tSNE map.

(C) Volcano plot demonstrates DEGs and non-DEGs between the pLN_1 and pLN_2 clusters. Color codes label upregulated DEGs. DEGs with a minimal percentage (min.pct) of <10% are not highlighted.

(D) Flow cytometric analysis of Ki67 expression in pLN, skin, and thymus Vγ6⁺ T cells. Left panel: Histogram shows the Ki67 expression of CD3⁺, γδTCR⁺, and Vγ6⁺ T cells. Right panel: Quantification of Ki67⁺ cells within the respective organ. Data are representative of two independent experiments, while each dot represents one mouse.

(E) BrdU labeling of Vγ6⁺ T cells. TcrdH2BeGFP mice were provided with BrdU in drinking water for 8–12 days. Left panel: Histogram shows the BrdU incorporation of CD3⁺, γδTCR⁺, and Vγ6⁺ T cells analyzed by flow cytometry. Right panel: Quantification of BrdU⁺ cells within the respective organ. Data are pooled from two independent experiments. One dot represents data of one mouse.

(legend continued on next page)

Scart1$^+$ Vγ6$^+$ T Cells Form Homogeneous but Distinct Subsets within Tissues

Next, we investigated the transcriptional programs reflecting tissue-specific adaptation of IL17-producing Vγ6$^+$ T cells and compared single-cell transcriptomes between Vγ6$^+$ $\gamma\delta$T17 cells derived from pLN, thymus, and skin. The tSNE plot of 641 thymus, 1,381 pLN, and 510 skin Vγ6$^+$ T cells depicted their clear separation into four cell clusters (Figure 3A). Skin and thymus Vγ6$^+$ T cells each formed only one unifying cell cluster, whereas pLN Vγ6$^+$ T cells segregated to one major (pLN_1) and one smaller cell cluster (pLN_2) (Figure 3A). We next investigated the proliferative capacity of Vγ6$^+$ T cells within the respective clusters. To this end, all Vγ6$^+$ T cells were scored based on the expression of genes enriched in G1, G2M, and S phase of the cell cycle, showing that these cells can undergo cell division (Figure 3B). However, besides the upregulated expression of genes related to DNA replication, such as *Top2a*, *Mki67*, and *Dnmt1* in cluster pLN_2, cells of both pLN clusters displayed, in general, highly similar gene expression programs (Figure 3C). Further flow cytometric analysis of Ki67 expression in Vγ6$^+$ T cells identified 20% of Vγ6$^+$ T cells as Ki67$^+$ within pLNs and thymus, whereas skin Vγ6$^+$ T cells showed low Ki67 expression (Figure 3D). Similarly, bromodeoxyuridine (BrdU) uptake of Vγ6$^+$ T cells pointed out that Vγ6$^+$ T cells in pLN and thymus have a higher proliferation rate than their skin counterparts (Figure 3E) (Haas et al., 2012; Sumaria et al., 2011). This is consistent with the idea that skin-resident Vγ6$^+$ T cells are terminally differentiated effector cells.

Next, we addressed transcriptional differences between pLN-, skin-, and thymus-derived Vγ6$^+$ $\gamma\delta$T17 cells through a detailed analysis of gene expression patterns. Although the identified cell clusters (pLN_1, pLN_2, Skin, and Thy) shared a number of common transcriptional programs, they clearly separated by specific DEGs (Figure 3F; Figure S5A; Table S1). These cluster-specific gene signatures were further reflected by differential expression of transcriptional regulators (e.g., *Klf2* in cluster pLN_1, *Rel* in skin; *Klf4* in thymocytes) (Figure S5B), as well as extracellular proteins (e.g., *Itgb1* or *Cd48* in both pLN clusters; *Icam1* in skin; *Ly6a* in thymocytes) (Figure S5C). Notably, all Vγ6$^+$ $\gamma\delta$T17 cells were identified as Scart1$^+$ (encoded by the gene *Cd163l1*) (Figure S5D), and Vγ6$^+$ $\gamma\delta$T17 cells from pLN and skin shared the same common (e.g., *Cd44* and *Ccr2*) and hitherto unidentified (e.g., *Amica1* and *Tmem176a/b*) signature genes, as described above for thymus (Figure S5D).

Next, we subjected all DEGs to KEGG (Kyoto Encyclopedia of Genes and Genomes) pathway analysis (Figure 3G). In line with the identification of proliferating Vγ6$^+$ T cells in pLNs (Figures 3B–3E), KEGG pathways related to cell cycle and DNA replication were enriched in the pLN_2 cluster. On the other hand, pathways linked to cellular activation and apoptosis were solely upregulated in the skin, whereas the term "IL-17 signaling pathway" was annotated to the thymocyte and skin clusters. Interestingly, no functional KEGG pathways were enriched in both pLN clusters, pointing to a non-effector phenotype of pLN Vγ6$^+$ T cells. Together, transcriptome analysis of thymus, pLN, and skin revealed that Scart1$^+$ Vγ6$^+$ T cells represent highly homogeneous cell clusters that are adapted to their respective tissue. Especially, the complementary data of Ki67$^+$ expression and BrdU$^+$ incorporation in Vγ6$^+$ T cells point to a higher proliferative capacity of pLN Vγ6$^+$ T cells as compared to skin Vγ6$^+$ T cells, which shows a uniform highly activated effector phenotype at the RNA level.

Skin $\gamma\delta$T17 Cells Show TCR Activation Profiles and an Effector Phenotype

Skin $\gamma\delta$ T cells are constantly exposed to environmental cues at the body surfaces (Nielsen et al., 2017). Here, single-cell RNA-seq identified genes involved in T cell activation (e.g., *Cd44*, *Cd69*, *Nr4a1*, *Il2ra*, *Itk*, and *Prr7*) and genes that transduce activation (*Phlda1*) to the TNFRSF (e.g., *Fas*, *Traf1*, *Tnfrsf9*, and *Phlda1*) and nuclear factor κB (NF-κB) (e.g., *Nfkbia*, *Nfkbid*, and *Rel*) pathway as upregulated in skin Vγ6$^+$ T cells (Figure 4A). Likewise, the recently identified negative regulator of $\alpha\beta$ T cell activation *Fam49b* (Shang et al., 2018) was downregulated in skin Vγ6$^+$ T cells (Figure 4A). To validate these findings, a side-by-side comparison of mRNA and protein expression levels of the selected genes reflecting T cell activation, namely *Cd44*, *Cd69*, and *Nr4a1* (Nur77), was performed (Figures 4B and 4C). Violin plots highlight high mRNA expression levels of *Cd44*, *Cd69*, and *Nr4a1* (Nur77) within the individual cells of the skin Vγ6$^+$ T cell cluster (Figure 4B; Table S1), while FACS analysis confirmed the higher expression of CD44, CD69, and CD25 by skin as compared to pLN and thymus Vγ6$^+$ T cells (Figure 4C) (Sumaria et al., 2011). In addition, we took advantage of a mouse model in which GFP is expressed under the control of the *Nr4a1* promoter (Zikherman et al., 2012). The *in vivo* analysis revealed highest Nur77 expression in skin $\gamma\delta$T17 cells (Figure 4C). As the immediate early activation gene Nur77 (*Nr4a1*) reflects antigen-receptor activation in B and T cells (Moran et al., 2011; Zikherman et al., 2012), we asked whether signals by the TCR drove the activation of effector functions in skin Vγ6$^+$ T cells. Indeed, skin and to some extent thymus, but not pLN Vγ6$^+$ T cells, expressed *Il17a* and *Il17f* mRNA under steady-state conditions (Figure 4D, top panel; Table S1). Of note, *Ifng* mRNA expression was found in none of the cells (Figure 4D, bottom panel; Table S1). Interestingly, mRNA of molecules mediating tissue regeneration like *Areg* (Amphiregulin) and *Tnfa* were also upregulated in the thymus and skin Vγ6$^+$ T cell clusters (Figure 4D, bottom panel; Table S1). Finally, we studied the IL-17A cytokine production capacity of pLN, skin, and thymus $\gamma\delta$ T cells by using IL-17A/IFN-γ double-reporter mice. Importantly, a considerable

(D and E) Bars represent median value. Statistic: not significant (ns) $p > 0.05$, *$p < 0.05$, **$p < 0.01$, ***$p < 0.001$, ****$p < 0.0001$ by one-way ANOVA and Tukey's honestly significant difference (HSD) test.

(F) Heatmap illustrates the top 15 upregulated DEGs within the pLN, skin, and thymus Vγ6$^+$ T cell clusters (scaled to logFC).

(G) KEGG pathways analysis of upregulated DEGs within the respective cluster. Here, only the most 10 enriched KEGG pathways of each Vγ6$^+$ T cell cluster are illustrated.

See also Figure S5 and Table S1.

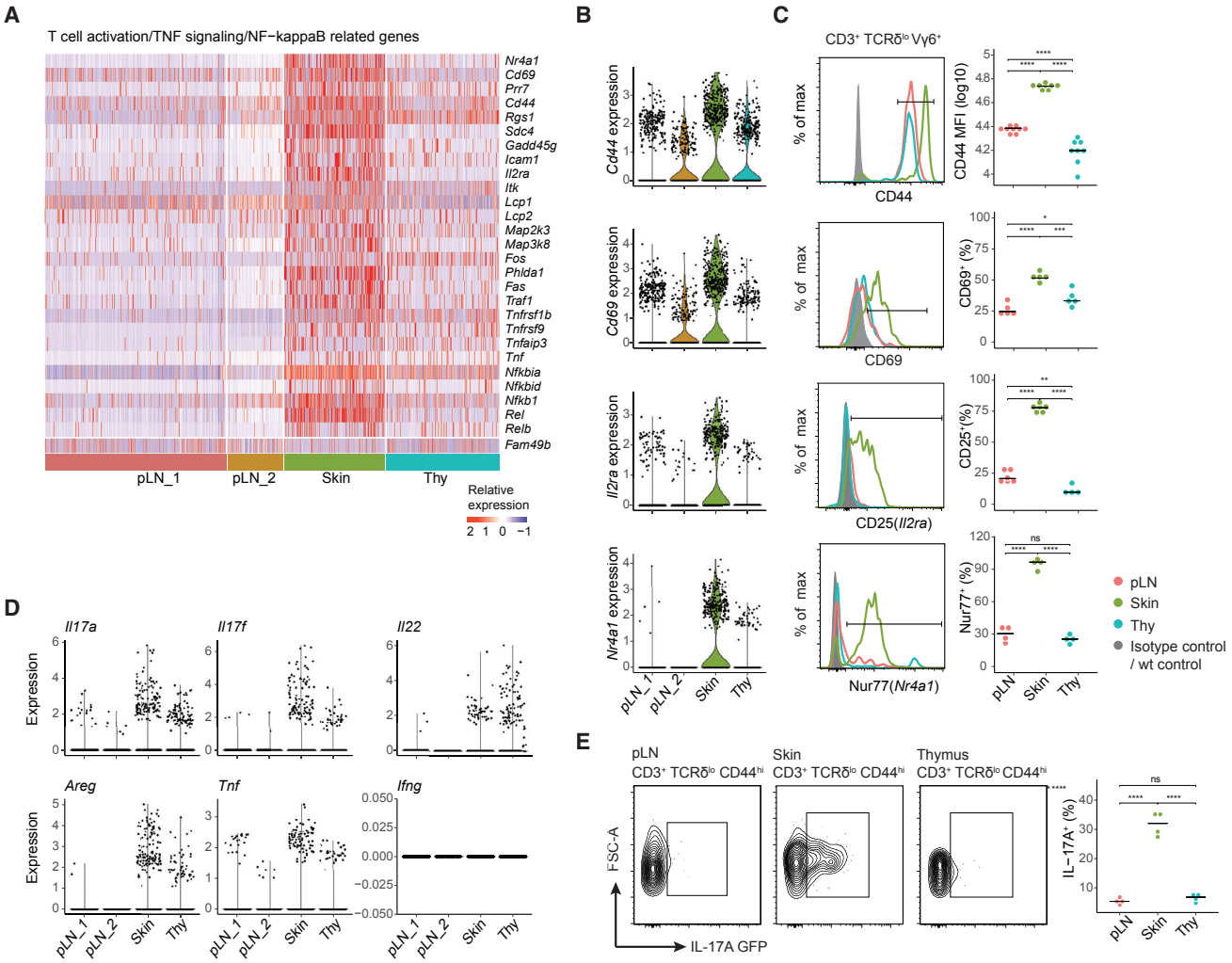

Figure 4. Skin Vγ6$^+$ γδ T Cells Are Highly Activated and Natural IL-17A Producers

(A) Expression of genes related to T cell activation, TNF receptors, and the NF-κB-signaling pathway within the Vγ6$^+$ T cell clusters (pLN1, pLN2, skin, and thymus). Expression values were scaled by logFC.

(B) Violin plots show normalized and log-transformed gene expression of *Cd44*, *Cd69*, *Cd25*, and *Nra4a1* within the Vγ6$^+$ T cell cluster.

(C) Flow cytometric analysis of identified DEGs. Histograms display the expression of corresponding genes shown in (B) on CD3$^+$, TCRδ$^+$, and Vγ6$^+$ T cells (left panel) and were quantified by dot plots (right panel). CD44, CD69, and CD25 were analyzed on C57BL/6 mice, and Nur77 expression was addressed in Nur77-GFP reporter mice.

(D) Violin plots represent expression levels of selected cytokine genes.

(E) Estimation of steady state IL-17A production in thymus, pLN, and skin γδT17 cells from Il17a-GFP/Ifng-YFP dual-reporter mice.

(C and E) The bars in scatterplots represent median value of each group. Statistic: not significant (ns) $p > 0.05$, *$p < 0.05$, **$p < 0.01$, ***$p < 0.001$, ****$p < 0.0001$ by one-way ANOVA and Tukey's HSD test. Data are representative of at least two or three independent experiments, while one dot represents one mouse.

See also Table S1.

fraction of skin CD44^{high} γδ T cells were GFP(IL-17A)$^+$ when analyzed directly *ex vivo* (30%), whereas IL-17A$^+$ γδ T cells were rarely present in thymus and pLN samples (Figure 4E). Notably, in both single-cell RNA-seq experiments the increase of *Il17a* in skin (avg_logFC = 1.05) was more significant than in thymus (avg_logFC = 0.30) (Table S1). This may explain the discrepancies between the RNA and protein levels for thymus Vγ6$^+$ T cells. In summary, these data suggest that dermal Vγ6$^+$ γδ T cells constantly receive activation signals by their TCR, which is reflected in upregulation of genes linked to T cell activation (*Nr4a1*) and molecules of the TNFRSF and NF-κB-signaling cascade. This leads to terminal effector differentiation of skin γδT17 cells, resulting in steady-state IL-17A production.

Functionally Differentiated Skin γδT17 Cells Are Protected from Apoptosis

It is conceivable that the chronic activation and the strong effector profile observed in skin Vγ6$^+$ T cells require a stringent

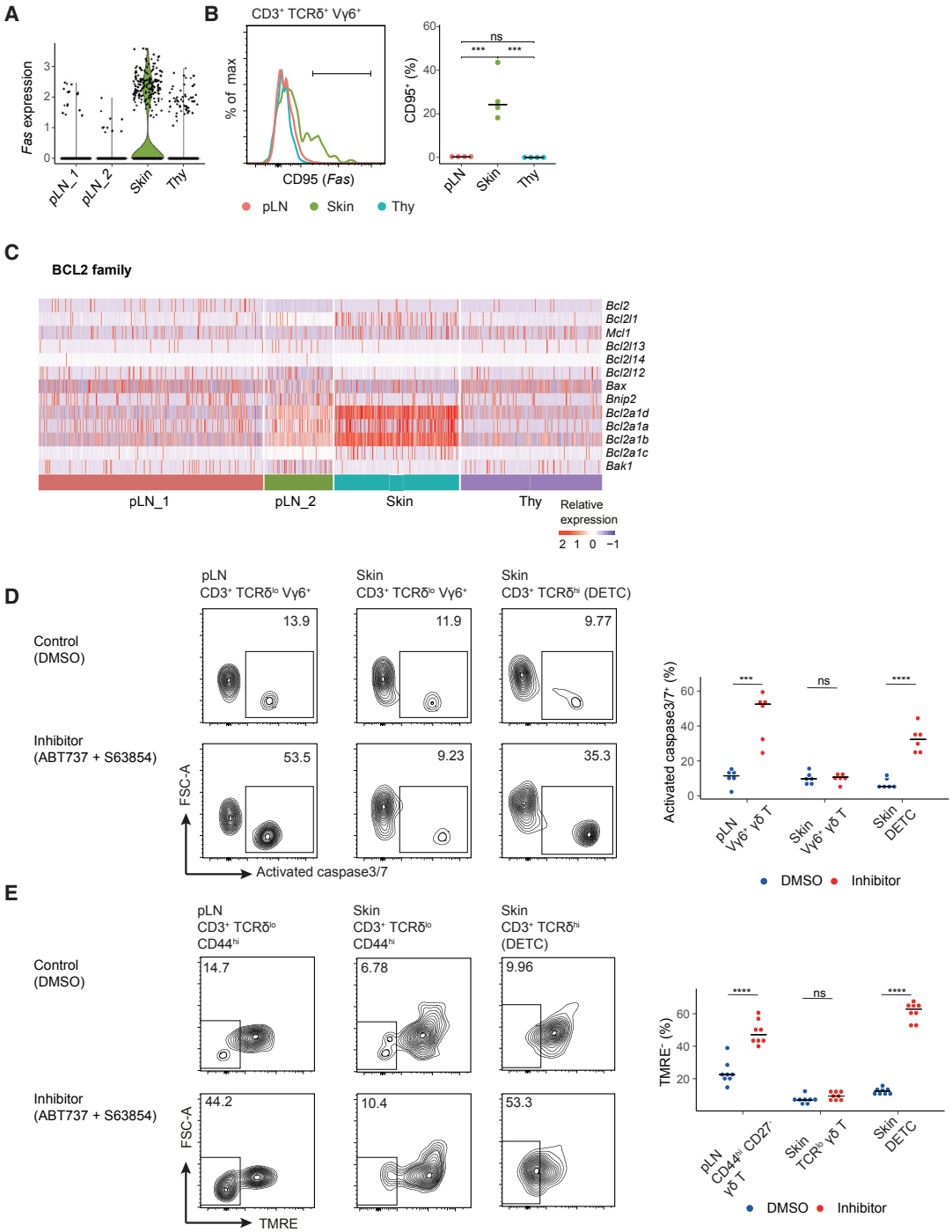

Figure 5. Functionally Differentiated Skin γδT17 Cells Are Protected from Apoptosis

(A) *Fas* expression within individual Vγ6$^+$ T cells of the pLN1, pLN2, skin, and thymus clusters.

(B) CD95 (*Fas*) protein expression on gated CD3$^+$, TCRδ$^+$, and Vγ6$^+$ T cells was analyzed by FACS, and mean values are illustrated as histograms and dot plots.

(C) Heatmap shows the expression of detected BCL2 family genes in the pLN1, pLN2, skin, and thymus Vγ6$^+$ T cell clusters. Gene expression levels were scaled to logFC.

(D and E) Lymphocytes of pLNs and skin were treated with DMSO (control) or BCL2 inhibitors, following analysis of (D) activated caspase-3/7 expression or (E) tetramethylrhodamine, ethyl ester (TMRE) by FACS.

(D) Contour plots illustrate activated caspase-3/7 CD3$^+$, γδTCR$^+$ and Vγ6$^+$ T cells or CD3$^+$, γδTCR^{high} DETCs. Activated caspase 3/7 expression was quantified by scatterplots.

(legend continued on next page)

regulation to ensure their longevity. Because activated skin Vγ6$^+$ T cells, showed at mRNA- and protein-level upregulation of the TNF-receptor CD95 (*Fas*) (Figures 5A and 5B), previously linked to activation-induced cell death in αβ T cells (Zhan et al., 2017), we wondered which cell-intrinsic factors mediated the long-term survival of skin γδT17 cells. To this end, we examined the expression of molecules regulating apoptotic cell death, such as the Bcl2 family members, which can have either pro-apoptotic (e.g., *Bax* and *Bim*) or anti-apoptotic functions (e.g., *Bcl2*, *Mcl-1*, and *Bcl2a1a-d*) (Carrington et al., 2017; Vogler, 2012). Of note, skin Vγ6$^+$ T cells showed high mRNA expression of *Bcl2a1a*, *b*, and *d* (Figure 5C; Table S1), which are direct targets of the NF-κB-signaling cascade and act as pro-survival factors (Vogler, 2012), while *Bcl2a1c* is a pseudogene (Hatakeyama et al., 1998). To address the functional relevance of anti-apoptotic proteins in skin γδT17 cell survival, apoptosis was induced in γδ T cells collected from pLN and skin of wild-type mice by treating them with a combination of two Bcl2-family inhibitors called ABT737 (inhibitor of Bcl2, Bcl-xl, and Bcl-w) and S63845 (inhibitor of Mcl-1) (Montero and Letai, 2018). Dysregulation of the Bcl2 family is fundamental to the pathophysiology of many hematologic malignancies (Valentin et al., 2018). Therefore, inhibitors targeting these pro-survival genes, called BH3 mimetics due to their selective binding to the BH3 domain of several members of the anti-apoptotic Bcl2 protein family, are potent inducers of mitochondrial apoptosis and, thus, used in targeting hematologic malignancies. After 3 h of co-incubation, cell death was determined through monitoring caspase3/7 activation by flow cytometry in Vγ6$^+$ T cells of pLN and skin (Figure 5D). In pLNs, cleaved caspase 3 was present in 23.74% (±4.99%) of cells treated with inhibitors, as compared to 8.17% (±1.44%) in DMSO-treated cells. Similar results were obtained for skin Vγ5$^+$ DETCs (12.53% ± 2.50% compared to 3.35% ± 0.99%) (Figure 5D). Importantly, activation of caspase3/7 did not significantly change in skin Vγ6$^+$ T cells incubated with DMSO or inhibitors (14.18% ± 6.60% to 14.41% ± 6.04%) (Figure 5D), indicating that skin Vγ6$^+$ T cells could be protected from apoptosis by Bcl2a1 proteins, as these were not affected by ABT-737 or S63845 treatment. At the same time, the mitochondrial outer membrane potential was determined by TMRE expression on all CD27$^-$, CD44^{high} Vγ6$^+$ T cells of pLN and skin as well as Vγ5$^+$ DETC treated with DMSO or Bcl2-family inhibitors (Figure 5E). In pLNs, the percentage of TMRE-negative CD44^{high} γδT17 was much higher (48.50% ± 7.32%) in inhibitor-treated cells than in DMSO controls (23.70% ± 7.20%), indicating membrane potential loss due to cellular apoptosis (Figure 5E). In contrast, skin γδT17 cells (9.62% ± 2.57%) or DMSO (7.14% ± 2.39%) but not Vγ5$^+$ DETCs (61.23% ± 5.76% [inhibitor] versus 12.28% ± 2.02% [DMSO]) showed similar TMRE expression in the presence of inhibitors (Figure 5E). In summary, we show that Bcl2a1 family proteins are specifically expressed in skin but not in thymus or pLN-derived γδT17 cells. Functionally, skin γδT17 cells were protected from Bcl2/Bcl-xl and Mcl-1 inhibitor-induced cell death, suggesting that other anti-apoptotic Bcl2 homologs, i.e., most likely Bcl2a1 proteins, ensure the survival and long-term maintenance of dermal effector γδT17 cells. However, in the steady state, mice lacking all functional Bcl2a1 proteins (Schenk et al., 2017) did not show reduced numbers and frequencies of γδT17 cells in dermis (Figure S6).

Skin Vγ6$^+$ and Vγ4$^+$ T Cells Are Highly Similar but Can Be Separated by Expression of Scart1 and Scart2

In contrast to Vγ4$^+$ γδ T cells in lymphatic organs, but similar to skin Vγ6$^+$ γδ T cells (Figure 4B), all skin Vγ4$^+$ γδ T cells are uniformly CD44^{high} (Figure 6A), thus pointing toward similar functional phenotypes of skin Vγ6$^+$ and Vγ4$^+$ γδT17 cells (Cai et al., 2011; Gray et al., 2011; Haas et al., 2012; Sumaria et al., 2011). To understand the molecular differences between skin Vγ4$^+$ and Vγ6$^+$ γδT17 cells, we generated an additional single-cell RNA-seq dataset comprising 864 sorted Vγ4$^+$ T cells isolated from ear skin (Figures S3B and S3C). Integrated analysis of these Vγ4$^+$ skin T cell single-cell transcriptomes together with the skin Vγ6$^+$ T cell library showed that Vγ6$^+$ and Vγ4$^+$ T cells form one unifying cluster (Figure 6B). Gene expression programs of skin Vγ6$^+$ and Vγ4$^+$ T cells were highly parallel and only a few DEGs (38 genes, average logFC > 0.5) could be identified, indicating that the two skin γδT17 cell subsets are functionally very similar (Figure 6C). Especially, gene signatures of skin γδT17 cells, such as *Cd69*, *Nr4a1* (Nur77), *Nfkb1*, *Bcl2a1d*, and *Sdc4*, but also of all mature activated γδT17 cells including *Cd44*, *Amica1*, and *Maf*, were detected in both groups (Figure 6D). Thus, independent of their expressed TCR γ-chain, all skin γδT17 cells displayed a surprisingly similar activated phenotype. Besides all parallels, identification of some DEGs determined so far unknown markers to distinguish skin Vγ4$^+$ and Vγ6$^+$ T cells. Only skin Vγ4$^+$ T cells were *5830411N06Rik* (Scart2) and *Cd9*-positive and showed higher *Lgals3* (Galectin-3) and *Il17f* expression, whereas *Cd163l1* (Scart1), *Ccr2*, *Pdcd1* (PD-1), and *Bcl2a1a* were more abundant in Vγ6$^+$ T cells (Figure 6E). Flow cytometric analysis confirmed that the inhibitory receptor PD-1 is expressed on a larger fraction of skin Vγ6$^+$ (79.2% ± 4.2%) compared to Vγ4$^+$ (14.6% ± 4.6%) T cells, thereby adding an additional level of regulation (Figure 6F). Finally Scart2, present on γδ T cells expressing IL-17 (Kisielow et al., 2008; Muzaki et al., 2017) and recently shown to identify pre-programmed Vγ4$^+$ γδT17 cells during intrathymic development (Spidale et al., 2018), was exclusively present on pLN, skin, and thymus Vγ6$^-$ T cells (Figure 6G), whereas skin Vγ6$^+$ T cells solely expressed mRNA of *Cd163l1* (Scart1) (Figure 6H). Overall, integrated analysis of skin γδT17 cells demonstrated overlapping functional phenotypes for both Vγ4$^+$ and Vγ6$^+$ γδT17 cells. However, mutually exclusive expression of Scart2 versus Scart1 distinguishes Vγ4$^+$ and Vγ6$^+$ γδT17 cells, possibly reflecting their distinct ontogenetic origin.

(E) TMRE expression was determined on CD44^{high}CD27$^-$ γδ T cells in pLN and skin or CD3$^+$, TCR^{low} skin DETCs and quantified by scatterplots.
(B, D, and E) Data are representative of two to three independent experiments using four to eight mice per experiment. Bars represent median value of each group. Statistic: ns p > 0.05, *p < 0.05, **p < 0.01, ***p < 0.001, ****p < 0.0001 by one-way ANOVA and Tukey's HSD test (B) or paired Student's t test.
See also Figure S6.

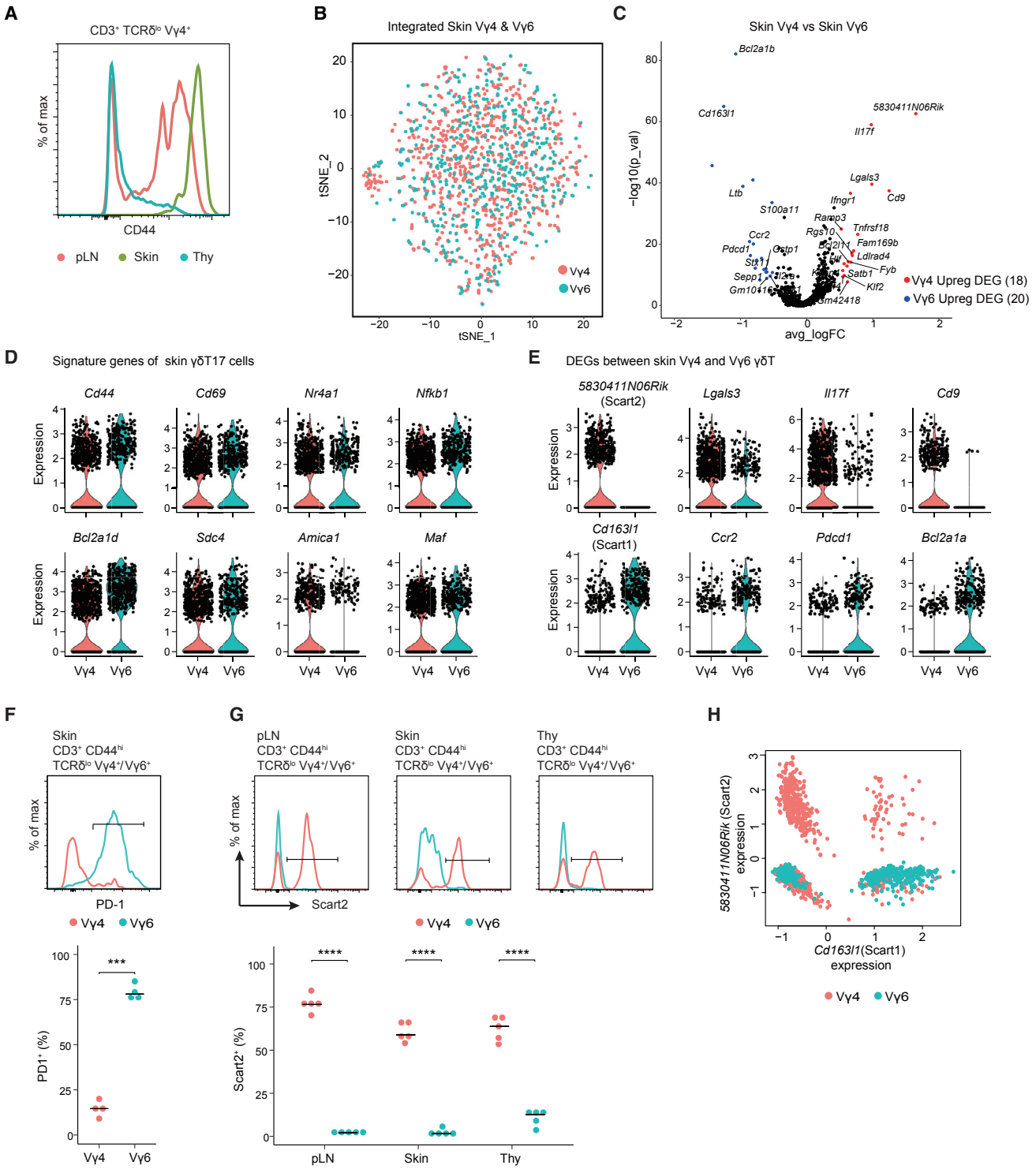

Figure 6. Skin Vγ6⁺ and Vγ4⁺ T Cells Are Highly Similar but Can Be Separated by Expression of Scart1 and Scart2

(A) Flow cytometry analysis to determine CD44 expression on Vγ4⁺ T cells in skin, pLN, and thymus. Data are representative of three independent experiments.

(B) Single-cell transcriptome libraries of skin Vγ4⁺ and skin Vγ6⁺ T cells were integrated by keeping library identity, following dimensional reduction analysis and tSNE visualization.

(C) Volcano plot shows similarities and differences between Vγ4⁺ and Vγ6⁺ T cells. Upregulated DEGs are color coded to either Vγ4⁺ (red) or Vγ6⁺ (blue) T cells. Most differentially expressed genes are shown on the plot.

(legend continued on next page)

DISCUSSION

Starting with the observation that Vγ6$^+$ γδT17 cells represented mostly tissue-resident effector cells in thymus, pLN, and skin, our study focused on the functional adaptation of Vγ6$^+$ γδT17 cells in the respective tissues at the single-cell level. We found that Vγ6$^+$ T cells formed highly homogeneous cell populations within adult thymus, pLNs, and skin that could be delineated by tissue-specific transcription programs. Surprisingly, pLN contained a separate cluster of Vγ6$^+$ T cells that was less prominently enriched for genes of the G1 phase. Furthermore, orthogonal data indicated a higher cell proliferation of pLN and thymus Vγ6$^+$ T cells than the skin. Supported by the findings that Vγ6$^+$ γδT17 cells are (1) fairly but not exclusively tissue resident, (2) have a higher motility than skin DETCs, and (3) can traffic between tissues under homeostatic conditions or inflammatory responses (Cai et al., 2014; Gray et al., 2011; Hartwig et al., 2015; McKenzie et al., 2017; Ramírez-Valle et al., 2015; Sandrock et al., 2018; Sumaria et al., 2011; Zhang et al., 2016), it is tempting to speculate that proliferating Vγ6$^+$ T cells in pLN and thymus provide a dormant reservoir for future tissue effector Vγ6$^+$ T cells. In other words, the less-activated CD69^{neg}, Vγ6$^+$ T cells in pLN and thymus are still capable of cell proliferation before undergoing their final differentiation to become tissue-specific effector Vγ6$^+$ T cells elsewhere. In line with our parabiosis experiments showing that the majority, but not all, of Vγ6$^+$ T cells display tissue residency, we propose that Vγ6$^+$ T cells from pLN and thymus can migrate to the skin and refill the pool of terminally differentiated skin Vγ6$^+$ T cells, which are PD1$^+$ and eventually undergo apoptosis after fulfilling their protective functions in the skin for a certain time. Further studies using disease models are needed to test this hypothesis.

In addition, our data suggest that the highly activated skin-screening effector γδT17 cells require a stringent regulation. Here, the strikingly specific and high expression of *Bcl2a1* proteins in skin-derived Vγ4$^+$ and Vγ6$^+$ γδT17 cells may ensure their persistence and longevity. Albeit γδ T cell numbers are reduced in the spleen of Bcl2a1 triple knockout mice (Schenk et al., 2017), dermal γδ T cells were not significantly affected under steady-state conditions, presumably due to compensatory effects by other anti-apoptotic proteins. So far, the anti-apoptotic family proteins Bcl2a1 have been described to be upregulated in a TCR-dependent manner during thymic development of γδT17 cells (Muñoz-Ruiz et al., 2016) and to protect human TCR-activated Vγ9Vδ2$^+$ γδ T cells from apoptosis (DeBarros et al., 2011) The latter studies are consistent with our observation that BH3 mimetics targeting all other anti-apoptotic proteins, including Bcl2, Bcl-xl, Bcl-w, and Mcl-1 but not the Bcl2a1 family, induced apoptosis in lymph-node-derived γδT17 cells and skin Vγ5$^+$ DETCs but not in skin γδT17 cells. Together, our data support the idea that effector γδT17 cells in the skin may specifically rely on the expression of anti-apoptotic Bcl2a1 proteins for protection from activation-induced cell death.

Our study further pointed out that TNFRSF- and NF-κB-signaling pathways are active in skin γδT17 cells, which is also reflected by increased Nur77 expression in skin Vγ6$^+$ γδT17 cells. Similar to tissue-resident Rorγt$^+$ αβ T cells (Vasanthakumar et al., 2017), these intracellular pathways might be TCR-dependent and critical for the tissue-specific function and homeostasis of skin Vγ6$^+$ γδT17 cells. Because ligands of human γδ T cells can comprise self-antigens or metabolic bi-products of microbial pathways (Adams et al., 2015), we hypothesize that either endogenous tissue-specific signals and/or the local microbiota are driving TCR-mediated activation pathways in the skin γδT17 cells (Muzaki et al., 2017; Wilharm et al., 2019). Akin, gene signatures of skin γδT17 cells were very similar to lymphoid TCR-activated γδ T cells (DeBarros et al., 2011; Muñoz-Ruiz et al., 2016). Moreover, the observed absence of *Lck* expression in γδT17 cells is in accordance with previous data showing that Lck is dispensable for the development and function of Vγ6Vδ1$^+$ T cells (Fujise et al., 1996) and Vγ4$^+$ T cells (Spidale et al., 2018), whereas the high *Lck* expression in single-cell transcriptomes of CD27$^+$ γδ thymocytes might reflect different TCR signaling pathways to become IFN-γ-producing γδ T cells (Jensen et al., 2008; Muñoz-Ruiz et al., 2016; Sumaria et al., 2017; Turchinovich and Hayday, 2011). Unlike CD27$^+$ γδ T cells, shown to immediately upregulate Nur77 upon *in vitro* TCR-stimulation, Vγ6$^+$ T cells in lymph nodes were rather slow responders to activation by their TCR (Wencker et al., 2014). In our study, transcriptome data suggested that skin γδT17 cells were chronically activated independent of Lck but possibly by their TCR, resulting in activation of the NF-κB-signaling pathway and *Il17a and Il17f* expression under steady-state conditions. It remains to be established whether γδT17 cells resident in other peripheral non-lymphoid (mucosal) tissues share similar gene expression programs with their skin counterparts.

The constant production of IL-17A highlights that skin-resident γδT17 cells have undergone a final functional differentiation into effector cells but may question the potential pro-inflammatory role of γδT17 cells under steady-state conditions (Papotto et al., 2018). Indeed, γδT17 cells were recently shown to mediate adipose tissue (Kohlgruber et al., 2018) and lung homeostasis (Guo et al., 2018) by the IL-17-IL-33 axis, and in the skin, IL-17A may induce IL-33 expression in keratinocytes. This, in turn, may promote Areg and IL-22 production by other skin-resident lymphocytes (Guo et al., 2018; Molofsky et al., 2015) and thereby regulate tissue-homeostasis. Likewise, gingival γδT17

(D and E) Signature genes of γδT17 cells (present in Vγ4$^+$ and Vγ6$^+$ T cells) (D) and selected DEGs between skin Vγ4$^+$ and Vγ6$^+$ T cells (E) are displayed by violin plots.

(F) PD-1 expression of skin Vγ4$^+$ and Vγ6$^+$ T cells was determined by flow cytometry. Scatterplot illustrates the quantification of PD-1$^+$ γδ T cells.

(G) Lymph node, skin, and thymus γδ T cells were analyzed for Scart2 expression by flow cytometry by gating on CD3$^+$, TCRδ^{low} and Vγ4$^+$, or Vγ6$^+$ T cells and quantified by dot plots.

(F and G) The bars represent the median value of each group. Statistic: ns $p > 0.05$, *$p < 0.05$, **$p < 0.01$, ***$p < 0.001$, ****$p < 0.0001$ by paired Student's t test. Data are representative of at least two independent experiments using four to five mice per experiment.

(H) Correlated mRNA expression of Scart1 and Scart2 on integrated Vγ4$^+$ and Vγ6$^+$ T cell datasets. Color codes indicate library identity (skin Vγ4$^+$ or Vγ6$^+$ T cells).

cells were shown to produce Areg to maintain oral barrier homeostasis (Krishnan et al., 2018). Interestingly, in our transcriptome data, mRNA of *Areg* was expressed in skin and thymus γδT17 cells but not in pLN γδT17 cells.

Finally, it is debatable whether these functions are specific for Vγ6$^+$ γδT17 cells. Although the Vγ6$^+$ TCR might be involved in the local activation of skin Vγ6$^+$ γδT17 cells, skin-resident Vγ4$^+$ T cells displayed extremely similar gene expression programs. Also, recent single-cell transcriptome data of other tissue-resident lymphocytes showed very complementary profiles (e.g., *Sdc4*, *Furin*, or *Gadd45b* expression) (Miragaia et al., 2019). Nevertheless, we observed some notable DEGs, coding for CD9, Galectin-3, and Scart2 as well as IL-17F in skin Vγ4$^+$ T cells and PD-1, Scart1, and IL-17A in skin Vγ6$^+$ γδT17 cells. This may guide different functionalities or homing capabilities. Regarding the mutually exclusive expression of Scart1 and Scart2 in Vγ6$^+$ T cells and Vγ4$^+$ T cells, respectively, we suggest that they could reflect an even earlier ontogenetic origin (Kisielow et al., 2011) of fetal-derived Vγ6$^+$ γδT17 cells, whereas Scart2 has been described as a marker of long-living Vγ4$^+$ γδT17 cells (Kisielow et al., 2008; Muzaki et al., 2017; Spidale et al., 2018).

STAR★METHODS

Detailed methods are provided in the online version of this paper and include the following:

- KEY RESOURCES TABLE
- CONTACT FOR REAGENT AND RESOURCE SHARING
- EXPERIMENTAL MODEL AND SUBJECT DETAILS
- METHOD DETAILS
  - Parabiosis
  - BrdU Assay
  - Single-cell suspension preparation
  - Flow cytometry and antibodies
  - BCL2 block and apoptosis measurement
  - Generation of single-cell RNA-seq libraries
  - Sequencing data processing
  - Cell clustering and differentially expressed genes profile
- QUANTIFICATION AND STATISTICAL ANALYSIS
- DATA AND SOFTWARE AVAILABILITY

SUPPLEMENTAL INFORMATION

Supplemental Information can be found online at https://doi.org/10.1016/j.celrep.2019.05.064.

ACKNOWLEDGMENTS

The work supported by Deutsche Forschungsgemeinschaft (DFG, German Research Foundation) under Germany's Excellence Strategy – EXC 2155 "RESIST" – Project ID 39087428 to S.R. and I.P.; SFB900 - Project ID 158989968 to S.R., C. Koenecke and I.P; SFB1192/A5 to C. Krebs and RA 3077/1-1 to S.R.; and the state of Lower Saxony COALITION (to S.R. and I.P.). L.T., I.O., J.B.-M., and A.W. were supported by the Hannover Biomedical Research School. We would like to acknowledge the assistance of the Cell Sorting Core Facility of the Hannover Medical School, and we thank Matthias Ballmaier for advice and Abdi Demera for animal care taking.

AUTHOR CONTRIBUTIONS

Conceptualization, L.T., I.S., I.P., and S.R.; Methodology, J.K., M.S.-S., M.J.H., C. Koenecke, A.-H.H., and C. Krebs; Formal Analysis, L.T.; Investigation, L.T., I.S., I.O. Y.A., A.W., J.B.-M., Y.T., A.B., T.A., and L.G.; Resources, J.K., M.S.-S., M.J.H., C. Koenecke, A.-H.H., and C. Krebs; Writing – Original Draft, I.P. and S.R.; Writing – Review & Editing, I.S., I.P., and S.R.; Visualization, L.T. and I.S.; Supervision, I.P. and S.R.

DECLARATION OF INTERESTS

The authors declare no conflict of interest.

Received: December 14, 2018
Revised: March 22, 2019
Accepted: May 17, 2019
Published: June 18, 2019

REFERENCES

Adams, E.J., Gu, S., and Luoma, A.M. (2015). Human gamma delta T cells: Evolution and ligand recognition. Cell. Immunol. *296*, 31–40.

Audemard-Verger, A., Rivière, M., Durand, A., Peranzoni, E., Guichard, V., Hamon, P., Bonilla, N., Guilbert, T., Boissonnas, A., Auffray, C., et al. (2017). Macrophages Induce Long-Term Trapping of γδ T Cells with Innate-like Properties within Secondary Lymphoid Organs in the Steady State. J. Immunol. *199*, 1998–2007.

Bauquet, A.T., Jin, H., Paterson, A.M., Mitsdoerffer, M., Ho, I.C., Sharpe, A.H., and Kuchroo, V.K. (2009). The costimulatory molecule ICOS regulates the expression of c-Maf and IL-21 in the development of follicular T helper cells and TH-17 cells. Nat. Immunol. *10*, 167–175.

Butler, A., Hoffman, P., Smibert, P., Papalexi, E., and Satija, R. (2018). Integrating single-cell transcriptomic data across different conditions, technologies, and species. Nat. Biotechnol. *36*, 411–420.

Cai, Y., Shen, X., Ding, C., Qi, C., Li, K., Li, X., Jala, V.R., Zhang, H.G., Wang, T., Zheng, J., and Yan, J. (2011). Pivotal role of dermal IL-17-producing γδ T cells in skin inflammation. Immunity *35*, 596–610.

Cai, Y., Xue, F., Fleming, C., Yang, J., Ding, C., Ma, Y., Liu, M., Zhang, H.G., Zheng, J., Xiong, N., and Yan, J. (2014). Differential developmental requirement and peripheral regulation for dermal Vγ4 and Vγ6T17 cells in health and inflammation. Nat. Commun. *5*, 3986.

Carding, S.R., and Egan, P.J. (2002). Gammadelta T cells: functional plasticity and heterogeneity. Nat. Rev. Immunol. *2*, 336–345.

Carrington, E.M., Zhan, Y., Brady, J.L., Zhang, J.G., Sutherland, R.M., Anstee, N.S., Schenk, R.L., Vikstrom, I.B., Delconte, R.B., Segal, D., et al. (2017). Anti-apoptotic proteins BCL-2, MCL-1 and A1 summate collectively to maintain survival of immune cell populations both in vitro and in vivo. Cell Death Differ. *24*, 878–888.

Ciofani, M., Madar, A., Galan, C., Sellars, M., Mace, K., Pauli, F., Agarwal, A., Huang, W., Parkhurst, C.N., Muratet, M., et al. (2012). A validated regulatory network for Th17 cell specification. Cell *151*, 289–303.

DeBarros, A., Chaves-Ferreira, M., d'Orey, F., Ribot, J.C., and Silva-Santos, B. (2011). CD70-CD27 interactions provide survival and proliferative signals that regulate T cell receptor-driven activation of human γδ peripheral blood lymphocytes. Eur. J. Immunol. *41*, 195–201.

Dent, A.L., Matis, L.A., Hooshmand, F., Widacki, S.M., Bluestone, J.A., and Hedrick, S.M. (1990). Self-reactive γδ T cells are eliminated in the thymus. Nature *343*, 714–719.

Dimova, T., Brouwer, M., Gosselin, F., Tassignon, J., Leo, O., Donner, C., Marchant, A., and Vermijlen, D. (2015). Effector Vγ9Vδ2 T cells dominate the human fetal γδ T-cell repertoire. Proc. Natl. Acad. Sci. USA *112*, E556–E565.

Fink, D.R., Holm, D., Schlosser, A., Nielsen, O., Latta, M., Lozano, F., and Holmskov, U. (2010). Elevated numbers of SCART1+ gammadelta T cells in

skin inflammation and inflammatory bowel disease. Mol. Immunol. *47*, 1710–1718.

Fujikado, N., Mann, A.O., Bansal, K., Romito, K.R., Ferre, E.M.N., Rosenzweig, S.D., Lionakis, M.S., Benoist, C., and Mathis, D. (2016). Aire Inhibits the Generation of a Perinatal Population of Interleukin-17A-Producing γδ T Cells to Promote Immunologic Tolerance. Immunity *45*, 999–1012.

Fujise, S., Matsuzaki, G., Kishihara, K., Kadena, T., Molina, T., and Nomoto, K. (1996). The role of p56lck in the development of gamma delta T cells and their function during an infection by Listeria monocytogenes. J. Immunol. *157*, 247–254.

Gray, E.E., Suzuki, K., and Cyster, J.G. (2011). Cutting edge: Identification of a motile IL-17-producing gammadelta T cell population in the dermis. J. Immunol. *186*, 6091–6095.

Gray, E.E., Ramírez-Valle, F., Xu, Y., Wu, S., Wu, Z., Karjalainen, K.E., and Cyster, J.G. (2013). Deficiency in IL-17-committed Vγ4(+) γδ T cells in a spontaneous Sox13-mutant CD45.1(+) congenic mouse substrain provides protection from dermatitis. Nat. Immunol. *14*, 584–592.

Guo, X.J., Dash, P., Crawford, J.C., Allen, E.K., Zamora, A.E., Boyd, D.F., Duan, S., Bajracharya, R., Awad, W.A., Apiwattanakul, N., et al. (2018). Lung gammadelta T Cells Mediate Protective Responses during Neonatal Influenza Infection that Are Associated with Type 2 Immunity. Immunity *49*, 531–544.6.

Haas, J.D., González, F.H., Schmitz, S., Chennupati, V., Föhse, L., Kremmer, E., Förster, R., and Prinz, I. (2009). CCR6 and NK1.1 distinguish between IL-17A and IFN-gamma-producing gammadelta effector T cells. Eur. J. Immunol. *39*, 3488–3497.

Haas, J.D., Ravens, S., Düber, S., Sandrock, I., Oberdörfer, L., Kashani, E., Chennupati, V., Föhse, L., Naumann, R., Weiss, S., et al. (2012). Development of interleukin-17-producing γδ T cells is restricted to a functional embryonic wave. Immunity *37*, 48–59.

Hamada, S., Umemura, M., Shiono, T., Tanaka, K., Yahagi, A., Begum, M.D., Oshiro, K., Okamoto, Y., Watanabe, H., Kawakami, K., et al. (2008). IL-17A produced by gammadelta T cells plays a critical role in innate immunity against listeria monocytogenes infection in the liver. J. Immunol. *181*, 3456–3463.

Hartwig, T., Pantelyushin, S., Croxford, A.L., Kulig, P., and Becher, B. (2015). Dermal IL-17-producing γδ T cells establish long-lived memory in the skin. Eur. J. Immunol. *45*, 3022–3033.

Hatakeyama, S., Hamasaki, A., Negishi, I., Loh, D.Y., Sendo, F., Nakayama, K., and Nakayama, K. (1998). Multiple gene duplication and expression of mouse bcl-2-related genes, A1. Int. Immunol. *10*, 631–637.

Hayday, A.C., Diamond, D.J., Tanigawa, G., Heilig, J.S., Folsom, V., Saito, H., and Tonegawa, S. (1985). Unusual organization and diversity of T-cell receptor alpha-chain genes. Nature *316*, 828–832.

Ilicic, T., Kim, J.K., Kolodziejczyk, A.A., Bagger, F.O., McCarthy, D.J., Marioni, J.C., and Teichmann, S.A. (2016). Classification of low quality cells from single-cell RNA-seq data. Genome Biol. *17*, 29.

In, T.S.H., Trotman-Grant, A., Fahl, S., Chen, E.L.Y., Zarin, P., Moore, A.J., Wiest, D.L., Zúñiga-Pflücker, J.C., and Anderson, M.K. (2017). HEB is required for the specification of fetal IL-17-producing γδ T cells. Nat. Commun. *8*, 2004.

Itohara, S., Farr, A.G., Lafaille, J.J., Bonneville, M., Takagaki, Y., Haas, W., and Tonegawa, S. (1990). Homing of a gamma delta thymocyte subset with homogeneous T-cell receptors to mucosal epithelia. Nature *343*, 754–757.

Jensen, K.D., Su, X., Shin, S., Li, L., Youssef, S., Yamasaki, S., Steinman, L., Saito, T., Locksley, R.M., Davis, M.M., et al. (2008). Thymic selection determines gammadelta T cell effector fate: antigen-naive cells make interleukin-17 and antigen-experienced cells make interferon gamma. Immunity *29*, 90–100.

Kashani, E., Föhse, L., Raha, S., Sandrock, I., Oberdörfer, L., Koenecke, C., Suerbaum, S., Weiss, S., and Prinz, I. (2015). A clonotypic Vγ4Jγ1/Vδ5Dδ2Jδ1 innate γδ T-cell population restricted to the CCR6^{+}CD27^{-} subset. Nat. Commun. *6*, 6477.

Kisielow, J., Kopf, M., and Karjalainen, K. (2008). SCART scavenger receptors identify a novel subset of adult gammadelta T cells. J. Immunol. *181*, 1710–1716.

Kisielow, J., Tortola, L., Weber, J., Karjalainen, K., and Kopf, M. (2011). Evidence for the divergence of innate and adaptive T-cell precursors before commitment to the αβ and γδ lineages. Blood *118*, 6591–6600.

Kohlgruber, A.C., Gal-Oz, S.T., LaMarche, N.M., Shimazaki, M., Duquette, D., Koay, H.F., Nguyen, H.N., Mina, A.I., Paras, T., Tavakkoli, A., et al. (2018). γδ T cells producing interleukin-17A regulate adipose regulatory T cell homeostasis and thermogenesis. Nat. Immunol. *19*, 464–474.

Kowalczyk, M.S., Tirosh, I., Heckl, D., Rao, T.N., Dixit, A., Haas, B.J., Schneider, R.K., Wagers, A.J., Ebert, B.L., and Regev, A. (2015). Single-cell RNA-seq reveals changes in cell cycle and differentiation programs upon aging of hematopoietic stem cells. Genome Res. *25*, 1860–1872.

Krishnan, S., Prise, I.E., Wemyss, K., Schenck, L.P., Bridgeman, H.M., McClure, F.A., Zangerle-Murray, T., O'Boyle, C., Barbera, T.A., Mahmood, F., et al. (2018). Amphiregulin-producing γδ T cells are vital for safeguarding oral barrier immune homeostasis. Proc. Natl. Acad. Sci. USA *115*, 10738–10743.

Lockhart, E., Green, A.M., and Flynn, J.L. (2006). IL-17 production is dominated by gammadelta T cells rather than CD4 T cells during Mycobacterium tuberculosis infection. J. Immunol. *177*, 4662–4669.

Lu, Y., Cao, X., Zhang, X., and Kovalovsky, D. (2015). PLZF Controls the Development of Fetal-Derived IL-17+Vγ6+ γδ T Cells. J. Immunol. *195*, 4273–4281.

Mair, F., Joller, S., Hoeppli, R., Onder, L., Hahn, M., Ludewig, B., Waisman, A., and Becher, B. (2015). The NFκB-inducing kinase is essential for the developmental programming of skin-resident and IL-17-producing γδ T cells. eLife *4*, e10087.

Malhotra, N., Narayan, K., Cho, O.H., Sylvia, K.E., Yin, C., Melichar, H., Rashighi, M., Lefebvre, V., Harris, J.E., Berg, L.J., and Kang, J.; Immunological Genome Project Consortium (2013). A network of high-mobility group box transcription factors programs innate interleukin-17 production. Immunity *38*, 681–693.

McKenzie, D.R., Kara, E.E., Bastow, C.R., Tyllis, T.S., Fenix, K.A., Gregor, C.E., Wilson, J.J., Babb, R., Paton, J.C., Kallies, A., et al. (2017). IL-17-producing γδ T cells switch migratory patterns between resting and activated states. Nat. Commun. *8*, 15632.

Miragaia, R.J., Gomes, T., Chomka, A., Jardine, L., Riedel, A., Hegazy, A.N., Whibley, N., Tucci, A., Chen, X., Lindeman, I., et al. (2019). Single-Cell Transcriptomics of Regulatory T Cells Reveals Trajectories of Tissue Adaptation. Immunity *50*, 493–504.e497.

Molofsky, A.B., Savage, A.K., and Locksley, R.M. (2015). Interleukin-33 in Tissue Homeostasis, Injury, and Inflammation. Immunity *42*, 1005–1019.

Montero, J., and Letai, A. (2018). Why do BCL-2 inhibitors work and where should we use them in the clinic? Cell Death Differ. *25*, 56–64.

Moran, A.E., Holzapfel, K.L., Xing, Y., Cunningham, N.R., Maltzman, J.S., Punt, J., and Hogquist, K.A. (2011). T cell receptor signal strength in Treg and iNKT cell development demonstrated by a novel fluorescent reporter mouse. J. Exp. Med. *208*, 1279–1289.

Muñoz-Ruiz, M., Ribot, J.C., Grosso, A.R., Gonçalves-Sousa, N., Pamplona, A., Pennington, D.J., Regueiro, J.R., Fernández-Malavé, E., and Silva-Santos, B. (2016). TCR signal strength controls thymic differentiation of discrete proinflammatory γδ T cell subsets. Nat. Immunol. *17*, 721–727.

Murphy, A.G., O'Keeffe, K.M., Lalor, S.J., Maher, B.M., Mills, K.H., and McLoughlin, R.M. (2014). Staphylococcus aureus infection of mice expands a population of memory γδ T cells that are protective against subsequent infection. J. Immunol. *192*, 3697–3708.

Muschaweckh, A., Petermann, F., and Korn, T. (2017). IL-1β and IL-23 Promote Extrathymic Commitment of CD27^{+}CD122^{-} γδ T Cells to γδT17 Cells. J. Immunol. *199*, 2668–2679.

Muzaki, A.R.B.M., Soncin, I., Setiagani, Y.A., Sheng, J., Tetlak, P., Karjalainen, K., and Ruedl, C. (2017). Long-Lived Innate IL-17-Producing γ/δ T Cells Modulate Antimicrobial Epithelial Host Defense in the Colon. J. Immunol. *199*, 3691–3699.

Narayan, K., Sylvia, K.E., Malhotra, N., Yin, C.C., Martens, G., Vallerskog, T., Kornfeld, H., Xiong, N., Cohen, N.R., Brenner, M.B., et al.; Immunological

Genome Project Consortium (2012). Intrathymic programming of effector fates in three molecularly distinct γδ T cell subtypes. Nat. Immunol. *13*, 511–518.

Nielsen, M.M., Witherden, D.A., and Havran, W.L. (2017). γδ T cells in homeostasis and host defence of epithelial barrier tissues. Nat. Rev. Immunol. *17*, 733–745.

Pantelyushin, S., Haak, S., Ingold, B., Kulig, P., Heppner, F.L., Navarini, A.A., and Becher, B. (2012). Rorγt+ innate lymphocytes and γδ T cells initiate psoriasiform plaque formation in mice. J. Clin. Invest. *122*, 2252–2256.

Papotto, P.H., Gonçalves-Sousa, N., Schmolka, N., Iseppon, A., Mensurado, S., Stockinger, B., Ribot, J.C., and Silva-Santos, B. (2017). IL-23 drives differentiation of peripheral γδ17 T cells from adult bone marrow-derived precursors. EMBO Rep. *18*, 1957–1967.

Papotto, P.H., Reinhardt, A., Prinz, I., and Silva-Santos, B. (2018). Innately versatile: γδ17 T cells in inflammatory and autoimmune diseases. J. Autoimmun. *87*, 26–37.

Petermann, F., Rothhammer, V., Claussen, M.C., Haas, J.D., Blanco, L.R., Heink, S., Prinz, I., Hemmer, B., Kuchroo, V.K., Oukka, M., and Korn, T. (2010). γδ T cells enhance autoimmunity by restraining regulatory T cell responses via an interleukin-23-dependent mechanism. Immunity *33*, 351–363.

Powolny-Budnicka, I., Riemann, M., Tänzer, S., Schmid, R.M., Hehlgans, T., and Weih, F. (2011). RelA and RelB transcription factors in distinct thymocyte populations control lymphotoxin-dependent interleukin-17 production in γδ T cells. Immunity *34*, 364–374.

Prinz, I., Sansoni, A., Kissenpfennig, A., Ardouin, L., Malissen, M., and Malissen, B. (2006). Visualization of the earliest steps of gammadelta T cell development in the adult thymus. Nat. Immunol. *7*, 995–1003.

Ramírez-Valle, F., Gray, E.E., and Cyster, J.G. (2015). Inflammation induces dermal Vγ4+ γδT17 memory-like cells that travel to distant skin and accelerate secondary IL-17-driven responses. Proc. Natl. Acad. Sci. USA *112*, 8046–8051.

Reinhardt, R.L., Liang, H.E., and Locksley, R.M. (2009). Cytokine-secreting follicular T cells shape the antibody repertoire. Nat. Immunol. *10*, 385–393.

Reinhardt, A., Ravens, S., Fleige, H., Haas, J.D., Oberdörfer, L., Łyszkiewicz, M., Förster, R., and Prinz, I. (2014). CCR7-mediated migration in the thymus controls γδ T-cell development. Eur. J. Immunol. *44*, 1320–1329.

Reinhardt, A., Yevsa, T., Worbs, T., Lienenklaus, S., Sandrock, I., Oberdörfer, L., Korn, T., Weiss, S., Förster, R., and Prinz, I. (2016). Interleukin-23-Dependent γ/δ T Cells Produce Interleukin-17 and Accumulate in the Enthesis, Aortic Valve, and Ciliary Body in Mice. Arthritis Rheumatol. *68*, 2476–2486.

Ribot, J.C., deBarros, A., Pang, D.J., Neves, J.F., Peperzak, V., Roberts, S.J., Girardi, M., Borst, J., Hayday, A.C., Pennington, D.J., and Silva-Santos, B. (2009). CD27 is a thymic determinant of the balance between interferon-gamma- and interleukin 17-producing gammadelta T cell subsets. Nat. Immunol. *10*, 427–436.

Roark, C.L., French, J.D., Taylor, M.A., Bendele, A.M., Born, W.K., and O'Brien, R.L. (2007). Exacerbation of collagen-induced arthritis by oligoclonal, IL-17-producing gamma delta T cells. J. Immunol. *179*, 5576–5583.

Rodríguez, C.I., Buchholz, F., Galloway, J., Sequerra, R., Kasper, J., Ayala, R., Stewart, A.F., and Dymecki, S.M. (2000). High-efficiency deleter mice show that FLPe is an alternative to Cre-loxP. Nat. Genet. *25*, 139–140.

Romagnoli, P.A., Sheridan, B.S., Pham, Q.M., Lefrançois, L., and Khanna, K.M. (2016). IL-17A-producing resident memory γδ T cells orchestrate the innate immune response to secondary oral Listeria monocytogenes infection. Proc. Natl. Acad. Sci. USA *113*, 8502–8507.

Sandrock, I., Reinhardt, A., Ravens, S., Binz, C., Wilharm, A., Martins, J., Oberdorfer, L., Tan, L., Lienenklaus, S., Zhang, B., et al. (2018). Genetic models reveal origin, persistence and non-redundant functions of IL-17-producing gammadelta T cells. J. Exp. Med *215*, 3006–3018.

Schenk, R.L., Tuzlak, S., Carrington, E.M., Zhan, Y., Heinzel, S., Teh, C.E., Gray, D.H., Tai, L., Lew, A.M., Villunger, A., et al. (2017). Characterisation of mice lacking all functional isoforms of the pro-survival BCL-2 family member A1 reveals minor defects in the haematopoietic compartment. Cell Death Differ. *24*, 534–545.

Shang, W., Jiang, Y., Boettcher, M., Ding, K., Mollenauer, M., Liu, Z., Wen, X., Liu, C., Hao, P., Zhao, S., et al. (2018). Genome-wide CRISPR screen identifies FAM49B as a key regulator of actin dynamics and T cell activation. Proc. Natl. Acad. Sci. USA *115*, E4051–E4060.

Sheridan, B.S., Romagnoli, P.A., Pham, Q.M., Fu, H.H., Alonzo, F., 3rd, Schubert, W.D., Freitag, N.E., and Lefrançois, L. (2013). γδ T cells exhibit multifunctional and protective memory in intestinal tissues. Immunity *39*, 184–195.

Shibata, K., Yamada, H., Hara, H., Kishihara, K., and Yoshikai, Y. (2007). Resident Vdelta1+ gammadelta T cells control early infiltration of neutrophils after Escherichia coli infection via IL-17 production. J. Immunol. *178*, 4466–4472.

Shibata, K., Yamada, H., Nakamura, R., Sun, X., Itsumi, M., and Yoshikai, Y. (2008). Identification of CD25+ gamma delta T cells as fetal thymus-derived naturally occurring IL-17 producers. J. Immunol. *181*, 5940–5947.

Shibata, K., Yamada, H., Sato, T., Dejima, T., Nakamura, M., Ikawa, T., Hara, H., Yamasaki, S., Kageyama, R., Iwakura, Y., et al. (2011). Notch-Hes1 pathway is required for the development of IL-17-producing γδ T cells. Blood *118*, 586–593.

Silva-Santos, B., Serre, K., and Norell, H. (2015). γδ T cells in cancer. Nat. Rev. Immunol. *15*, 683–691.

Spidale, N.A., Sylvia, K., Narayan, K., Miu, B., Frascoli, M., Melichar, H.J., Zhihao, W., Kisielow, J., Palin, A., Serwold, T., et al. (2018). Interleukin-17 Producing gammadelta T Cells Originate from SOX13(+) Progenitors that Are Independent of gammadeltaTCR Signaling. Immunity *49*, 857–872.e5.

Sumaria, N., Roediger, B., Ng, L.G., Qin, J., Pinto, R., Cavanagh, L.L., Shklovskaya, E., Fazekas de St Groth, B., Triccas, J.A., and Weninger, W. (2011). Cutaneous immunosurveillance by self-renewing dermal gammadelta T cells. J. Exp. Med. *208*, 505–518.

Sumaria, N., Grandjean, C.L., Silva-Santos, B., and Pennington, D.J. (2017). Strong TCRγδ Signaling Prohibits Thymic Development of IL-17A-Secreting γδ T Cells. Cell Rep. *19*, 2469–2476.

Sutton, C.E., Lalor, S.J., Sweeney, C.M., Brereton, C.F., Lavelle, E.C., and Mills, K.H. (2009). Interleukin-1 and IL-23 induce innate IL-17 production from gammadelta T cells, amplifying Th17 responses and autoimmunity. Immunity *31*, 331–341.

Turchinovich, G., and Hayday, A.C. (2011). Skint-1 identifies a common molecular mechanism for the development of interferon-γ-secreting versus interleukin-17-secreting γδ T cells. Immunity *35*, 59–68.

Valentin, R., Grabow, S., and Davids, M.S. (2018). The rise of apoptosis: targeting apoptosis in hematologic malignancies. Blood *132*, 1248–1264.

Vasanthakumar, A., Liao, Y., Teh, P., Pascutti, M.F., Oja, A.E., Garnham, A.L., Gloury, R., Tempany, J.C., Sidwell, T., Cuadrado, E., et al. (2017). The TNF Receptor Superfamily-NF-κB Axis Is Critical to Maintain Effector Regulatory T Cells in Lymphoid and Non-lymphoid Tissues. Cell Rep. *20*, 2906–2920.

Vermijlen, D., and Prinz, I. (2014). Ontogeny of Innate T Lymphocytes - Some Innate Lymphocytes are More Innate than Others. Front. Immunol. *5*, 486.

Vogler, M. (2012). BCL2A1: the underdog in the BCL2 family. Cell Death Differ. *19*, 67–74.

Wei, Y.L., Han, A., Glanville, J., Fang, F., Zuniga, L.A., Lee, J.S., Cua, D.J., and Chien, Y.H. (2015). A Highly Focused Antigen Receptor Repertoire Characterizes γδ T Cells That are Poised to Make IL-17 Rapidly in Naive Animals. Front. Immunol. *6*, 118.

Wencker, M., Turchinovich, G., Di Marco Barros, R., Deban, L., Jandke, A., Cope, A., and Hayday, A.C. (2014). Innate-like T cells straddle innate and adaptive immunity by altering antigen-receptor responsiveness. Nat. Immunol. *15*, 80–87.

Wilharm, A., Tabib, Y., Nassar, M., Reinhardt, A., Mizraji, G., Sandrock, I., Heyman, O., Barros-Martins, J., Aizenbud, Y., Khalaileh, A., et al. (2019). Mutual interplay between IL-17-producing γδT cells and microbiota orchestrates oral mucosal homeostasis. Proc. Natl. Acad. Sci. USA *116*, 2652–2661.

Witherden, D.A., Verdino, P., Rieder, S.E., Garijo, O., Mills, R.E., Teyton, L., Fischer, W.H., Wilson, I.A., and Havran, W.L. (2010). The junctional adhesion molecule JAML is a costimulatory receptor for epithelial gammadelta T cell activation. Science *329*, 1205–1210.

Yu, G., Wang, L.G., Han, Y., and He, Q.Y. (2012). clusterProfiler: an R package for comparing biological themes among gene clusters. OMICS *16*, 284–287.

Zeng, X., Wei, Y.L., Huang, J., Newell, E.W., Yu, H., Kidd, B.A., Kuhns, M.S., Waters, R.W., Davis, M.M., Weaver, C.T., and Chien, Y.H. (2012). γδ T cells recognize a microbial encoded B cell antigen to initiate a rapid antigen-specific interleukin-17 response. Immunity *37*, 524–534.

Zhan, Y., Carrington, E.M., Zhang, Y., Heinzel, S., and Lew, A.M. (2017). Life and Death of Activated T Cells: How Are They Different from Naïve T Cells? Front. Immunol. *8*, 1809.

Zhang, B., Wu, J., Jiao, Y., Bock, C., Dai, M., Chen, B., Chao, N., Zhang, W., and Zhuang, Y. (2015). Differential Requirements of TCR Signaling in Homeostatic Maintenance and Function of Dendritic Epidermal T Cells. J. Immunol. *195*, 4282–4291.

Zhang, Y., Roth, T.L., Gray, E.E., Chen, H., Rodda, L.B., Liang, Y., Ventura, P., Villeda, S., Crocker, P.R., and Cyster, J.G. (2016). Migratory and adhesive cues controlling innate-like lymphocyte surveillance of the pathogen-exposed surface of the lymph node. eLife *5*, e18156.

Zikherman, J., Parameswaran, R., and Weiss, A. (2012). Endogenous antigen tunes the responsiveness of naive B cells but not T cells. Nature *489*, 160–164.

Zuberbuehler, M.K., Parker, M.E., Wheaton, J.D., Espinosa, J.R., Salzler, H.R., Park, E., and Ciofani, M. (2019). The transcription factor c-Maf is essential for the commitment of IL-17-producing γδ T cells. Nat. Immunol. *20*, 73–85.

STAR★METHODS

KEY RESOURCES TABLE

REAGENT or RESOURCE	SOURCE	IDENTIFIER
Antibodies		
Brilliant Violet 711 anti-mouse CD3ε Antibody	Biolegend	Cat#100349; RRID:AB_2565841
Brilliant Violet 605 anti-mouse CD3ε Antibody	Biolegend	Cat#100351; RRID:AB_2565842
PE/Cy7 anti-mouse CD3ε Antibody	Biolegend	Cat#100320; RRID:AB_312685
PerCP/Cy5.5 anti-mouse CD95 (Fas) Antibody	Biolegend	Cat#152610; RRID:AB_2632905
Brilliant Violet 605 anti-mouse CD69 Antibody	Biolegend	Cat#104529; RRID:AB_11203710
PerCP/Cy5.5 anti-mouse CD69 Antibody	Biolegend	Cat#104522; RRID:AB_2260065
PerCP/Cy5.5 anti-mouse/rat/human CD27 Antibody	Biolegend	Cat#123214; RRID:AB_2275577
Brilliant Violet 711 anti-mouse Ly-6A/E Antibody	Biolegend	Cat#108131; RRID:AB_2562241
Alexa Fluor® 647 anti-mouse JAML Antibody	Biolegend	Cat# 128506; RRID:AB_1186014
Brilliant Violet 711 anti-mouse/human CD44 Antibody	Biolegend	Cat#103057; RRID:AB_2564214
Zombie Aqua Fixable Viability Kit	Biolegend	Cat#423102
APC Anti-mouse TCR γ/δ Antibody	Biolegend	Cat#118116; RRID:AB_1731813
Anti-CD44-VioBlue, mouse	Miltenyi biotec	Order no: 130-116-495; RRID:AB_2727570
CD45.2-VioGreen, mouse	Miltenyi biotec	Order no: 130-102-312; RRID:AB_2660725
Anti-TCRβ-APC-Vio770, mouse	Miltenyi biotec	Order no:130-104-811; RRID:AB_2654026
Anti-TCRβ-PerCP-Vio700, mouse	Miltenyi biotec	Order no:130-104-816; RRID:AB_2654028
Anti-TCRγ/δ-PE-Vio770, mouse	Miltenyi biotec	Order no: 130-104-010; RRID:AB_2654084
Anti-Ki-67-PE-Vio770, human and mouse	Miltenyi biotec	Order no: 130-100-291; RRID:AB_2752141
PE-CF594 Hamster Anti-Mouse CD279	BD Bioscience	Cat#562523; RRID:AB_2737634
BD PharMingen PerCP-Cy5.5 Rat Anti-Mouse CD25	BD Bioscience	Cat#551071; RRID:AB_394031
CD45.1 Monoclonal Antibody (A20), PerCP-Cyanine5.5	ThermoFisher	Cat#45-0453-82; RRID:AB_2534955
IgM Monoclonal Antibody (RM-7B4), PE	ThermoFisher	Cat#12-434282; RRID:AB_10668833
anti-Tcr-Vγ4 (clone: UC3-10A6)	homemade	Dent et al., 1990
anti-Tcr-Vγ5/Vγ6 (clone: 17D1)	homemade	Roark et al., 2007
anti-Scart-2 (clone: 25A2)	homemade	Kisielow et al., 2008
anti-TCRγ/δ-unlabeled (clone: GL3)	homemade	N/A
anti-CD4 IgM (M31)	homemade	N/A
anti-CD8 IgM (RL1.72)	homemade	N/A
anti-CD4-biotin (clone RMCD4-2)	homemade	N/A
anti-CD8β-biotin (RMCD8)	homemade	N/A
Anti-FcR Antibody	homemade	cell culture supernatant
Chemicals, Peptides, and Recombinant Proteins		
Foxp3 / Transcription Factor Staining Buffer Set	ThermoFisher	Cat#00-5523-00
CellEvent Caspase-3/7 Green Reagent solution	ThermoFisher	Cat#C10423
Collagenase IV	Worthington	Cat#LS004188
DNase I, grade II	Roche	Cat#10104159001
Standard Rabbit Complement	Cederlane	Cat#CL3120
Lympholyte®-M Cell Separation Media	Cederlane	Cat#CL5035
Percoll®	Sigma-Aldrich	Cat#P4937-500ML
ABT-737	Selleck Chemicals	Cat#S1002
S63845	Selleck Chemicals	Cat#S8383
TMRE-Mitochondrial Membrane Potential Assay Kit	Abcam	Cat#ab113852

(*Continued on next page*)

Continued

REAGENT or RESOURCE	SOURCE	IDENTIFIER
Chromium Single Cell 3′ reagent kits v2	10xGenomics	Cat#120267
Streptavidin Microbeads	Miltenyi biotec	Order no:130-048-101
Deposited Data		
Data files for single cell RNA sequencing	This paper	GSE123400
Experimental Models: Organisms/Strains		
mouse: C57BL/6NCrl	Charles River	N/A
mouse: C57BL/6-Trdc^{tm1Mal}	Prinz et al., 2006	JAX ID 016941
mouse: B6.FVB(Cg)-Tg(Nr4a1-EGFP)GY139Gsat	Zikherman et al., 2012	N/A
mouse: IFNγ/IL17A-dual-reporter mice (B6.129S4-*Ifng*$^{tm3.1Lky}$ x B6.129S4-*Il17a*^{tm1Bcgen})	Laboratory of Bruno Silva-Santos	JAX ID 017581 x JAX ID 018472
mouse: B6.129S-Tcrd$^{tm1.1(cre/ERT2)Zhu}$/J	Zhang et al., 2015	JAX ID 031679
mouse: CD45.2+ C57BL/6	Harlan Laboratories (Rehovot, Isreal)	N/A
mouse: CD45.1+ C57BL/6	Jackson Laboratory	JAX ID 002014
mouse: C57BL/6-A1$^{-/-}$	Schenk et al., 2017	N/A
mouse: B6;SJL-Tg(ACTFLPe)9205Dym/J	Rodríguez et al., 2000	JAX ID005703
Software and Algorithms		
Seurat v2.3	Butler et al., 2018	https://satijalab.org/seurat/
Cell Ranger v2.2	10xGenomics	https://support.10xgenomics.com/
clusterProfiler	Yu et al., 2012	https://github.com/GuangchuangYu/clusterProfiler
FlowJo10.0	FlowJo, LLC	https://www.flowjo.com

CONTACT FOR REAGENT AND RESOURCE SHARING

Further information and requests for resources and reagents should be directed to and will be fulfilled by the Lead Contact, Sarina Ravens (ravens.sarina@mh-hannover.de).

EXPERIMENTAL MODEL AND SUBJECT DETAILS

We used C57BL/6NCrl mice, C57BL/6-*Trdc*^{tm1Mal} (here Tcrd-H2BEGFP) mice (Prinz et al., 2006), B6.129S-Tcrd$^{tm1.1(cre/ERT2)Zhu}$/J (here Tcrd^{CreEr}) mice (Zhang et al., 2015), B6;SJL-Tg(ACTFLPe)9205Dym/J (here ACT-FLPe) mice (Rodríguez et al., 2000), and B6.FVB(Cg)-Tg(*Nr4a1*-EGFP)GY139Gsat (here Nur77-GFP) mice (Zikherman et al., 2012).

The IFNγ/IL-17A-dual-reporter mice were obtained by crossing B6.129S4-*Ifng*$^{tm3.1Lky}$ (Reinhardt et al., 2009) and B6.129S4-*Il17a*^{tm1Bcgen} mice (purchased form Biocytgen, BcG-0001) and Bcl2a1 triple-knock-out mice (C57BL/6-A1$^{-/-}$) have been described previously (Schenk et al., 2017). For all experiments adult mice of both genders were used and allocated randomly to the experimental groups. Mice were kept under specific pathogen free conditions in the central animal facility at Hannover Medical School. For dissection of organs and preparation of single cell suspensions mice were sacrificed by CO_2-inhalation and cervical dislocation. All experimental procedures were conducted according to institutional guidelines approved by Lower Saxony State Office for Consumer Protection and Food safety animal care and use committee (reference number 33.19-42502-04-17/2704).

For parabiosis experiments 12 weeks old male CD45.2$^+$ and CD45.1$^+$ C57BL/6 mice were used. Mice were housed in the same cage for two weeks before the surgery. After surgery mice were maintained on a soft diet. The Hebrew University Institutional Animal Care and Use Committee approved the used parabiosis protocol (approval number MD-17-15356-5)

METHOD DETAILS

Parabiosis

For parabiosis surgery lateral skin incisions were made from elbow to knee in each mouse, forelimbs and hind limbs were tied together using nylon suture, and the skin incisions were closed using stainless steel wound clips. Blood exchange was confirmed 14 days after parabiosis by examining B cell chimerism using flow cytometry. Tissues were collected 4 weeks after the surgery in order to assess γδ T cells. The percentage of host cells in a given T cell subset corresponds to the percentage of CD45.1$^+$ cells for the CD45.1 and the percentage of CD45.2$^+$ cells for the CD45.2 parabiont.

BrdU Assay

BrdU was administered to the drinking water at a concentration of 0.8 mg BrdU / ml. Mice were analyzed after 8 – 12 days with BrdU-supplemented drinking water. BrdU staining of indicated organs was performed using BD Pharming BrdU Flow Kit (BD Biosciences) according to manufactures instructions.

Single-cell suspension preparation

To isolate lymphocytes from ear skin, ears were split into dorsal and ventral layers, cut into small pieces, and digested in RPMI media supplemented with (2mg/ml) collagenase IV (Worthington) and (187.5 μg/ml) DNaseI (Roche) for 75 minutes at 37°C under 1400 rpm of shaking. After stopping the digestion with 5mM EDTA, ears were further dissociated via a 18G needle. Next, cells were filtered through a 100 μM cell strainer (Falcon) for density gradient centrifugation using 40% and 70% Percoll solutions and re-suspended in MACS buffer (PBS with 3% FCS and 4mM EDTA).

Single cell suspensions from thymus and pLNs (including superficial cervical, axillary, brachial and inguinal lymph nodes) were obtained by filtering organs through nylon gaze. Thymus samples were depleted for $CD4^+$ and $CD8^+$ T cells in two ways: For single cell transcriptome library generation of FACS-sorted $V\gamma6^+$ T cell, $CD4^+$ and/or $CD8^+$ thymus cells were lysed via incubation with monoclonal anti-CD4 and anti-CD8β IgM (homemade), DNaseI (Roche) and Standard Rabbit Complement (Cederlane) at 37°C for 30 minutes. Next, thymus cells were retrieved via Lympholyte M (Cederlane) density gradient centrifugation. For all flow cytometric analysis experiments, thymocytes were incubated with biotinylated anti-CD4 and anti-CD8β antibodies (homemade). After washing, re-suspended cells were incubated with Streptavidin MicroBeads (Miltenyi Biotec) and non-labeled cells were isolated via autoMACS (Miltenyi Biotec) separation according to the manufacturer guidelines.

Flow cytometry and antibodies

Fc-receptors were blocked with FcR antibody (clone 2.4G2). The antibodies CD3ε (clone 145-2C11), CD95 (clone 5A367H8), CD69 (clone H1.2F3), CD27 (clone LG3A10), Ly6a (clone D7), JAML (clone 4E10) and CD44 (clone IM7) and Zombie Aqua Fixable Viability Kit, all purchased from Biolegend, and Tcrβ (clone: REA38), CD44 (IM7.8.1) and Ki67 (clone: B56), purchased from Miltenyi biotec, PD-1 (clone: J43) and anti-rat IgM (clone: RM-7B4), CD25 (clone: PC61), purchased from BD Bioscience, were used in this study. The anti-Tcrδ (clone: GL3), anti-Vγ4 (clone: UC3-10A6), anti-Vγ5/γ6 (clone: 17D1) antibodies were homemade. The anti-Scart-2 (clone: 25A2) has been described previously (Kisielow et al., 2008). The Vγ6 staining was done according to Haas et al. (2012). Briefly, after pre-incubation with unlabeled GL3 antibody, the anti-Vγ5/6 antibody was added to subsequently stain with anti-IgM-PE. For intracellular Ki67 staining the Foxp3/Transcription Factor Staining Buffer Set (eBioscience) was used. LSR II (BD Bioscience) was employed for flow cytometry. For flow cytometry data, we analyzed and visualized the data by FlowJo10.0, R package ggplot2, ggpubr and rstatix.

BCL2 block and apoptosis measurement

In order to block BCL2, cells ($\leq 3*10^6$ cells/mL) were incubated with 1.6 μM of ABT737 (Selleck Chemicals) together with 0.8 μM of S63845 (Selleck Chemicals) or 0.2% DMSO for 3 hours at 37°C. Apoptosis was assessed by using (i) CellEvent Caspase-3/7 Green Reagent assay (ThermoFisher) or (ii) mitochondrial transmembrane potential assay (TMRE, Abcam) according to the manufactures recommendations.

Generation of single-cell RNA-seq libraries

FACS-Aria II (BD Bioscience) was used for cell sorting of indicated cell populations into PBS/4mM EDTA/5%FCS. Sorted cells were diluted to $\leq$ 1000 cells/μL. Single cell sequencing libraries were generated using the Chromium Single Cell 3′ reagent kits v2 according to the manufactures protocol (10xGenomics). Indexed libraries were pooled, and paired-end sequencing was performed (Hiseq4000/Illumina).

Sequencing data processing

Sequence reads were aligned to the reference mouse genome mm10 (UCSC), following generation of barcode-gene matrices via Cell Ranger v2.0 (10xGenomics). Data from ambient RNA was trimmed based on nUMI-barcode saturation curve.

Cell clustering and differentially expressed genes profile

The R package Seurat v2.3 was used under R v3.5 for data trimming, unsupervised clustering and visualization (Butler et al., 2018). Briefly, to remove cells with poor sequence read quality, doublets and stressed cells, genes expressed on less than 10 cells and cells that had a gene number lower 400 or higher than 2500 were removed. Mitochondrial gene ratio was calculated to filter out cells with more than 8% mitochondrial genes (Ilicic et al., 2016). Next, the function 'NormalizeData' was applied to normalize for differences on sequencing depth across single cells. Cell cycle score and cell phases were assigned by the function 'CellCycleScoring' according to a gene list of cell cycle markers (Kowalczyk et al., 2015). To reduce confounders, UMI number, percentage of mitochondrial genes and cell cycle scores were regressed out by the function 'ScaleData'. Highly variable genes (hvg) were defined by 'FindVariableGenes' and used as input for principle component analysis (PCA). Using the PCElbowplot, we determined principle components (PCs) as statistically significant PCs which explained the most variance, while the PCs containing high ratio

of mitochondrial genes and ribosome genes were excluded as unwanted sources of heterogeneity. Based on significant PCs and setting resolution = 0.4, unsupervised graph-based clustering was performed by 'FindCluster'. Cells are embedded by tSNE plot. We executed 'FindAllMarkers' to identify differentially expressed genes (DEGs) among all genes, surface markers (Gene ontology term 0009986), or transcription factors (Riken Transcription Factor Database) by using wilcoxon rank sum test. We defined DEGs as average log2-fold change (logFC) $\geq$ 0.5, expressed in minimal percentage cells in at least 1 test group (min.pct) $\geq$ 20%, and adjust p value $\leq$ 0.01.

Libraries of thymus, skin and pLN Vγ6$^+$ T cells were aggregated and normalized by 'cellranger aggr' command provided by Cell Ranger. For dataset cleaning and indentification of IL-17-committed $\gamma\delta$ T cells, Immune signature module scores were added to each cell by 'AddModuleScore' function according to lists of known markers of IL-17-committed $\gamma\delta$ T cells and immature $\gamma\delta$ T cells (Figure S3B). Clusters with high $\gamma\delta$17 scores and low immature scores were subdivided as Vγ6$^+$ T cell dataset to analyze and cluster as described above.

The datasets from two independent experiments were further aggregated for reproducibility validation.

To find out the connection between gene signatures and functionalities, Kyoto Encyclopedia of Genes and Genomes (KEGG) pathway enrichment analysis was performed by the R package 'clusterProfiler' based on the upregulated DEGs in each Vγ6$^+$ T clusters (Yu et al., 2012). We set p value cutoff = 0.05 for significant enriched terms.

To compare the transcriptome of skin Vγ4$^+$ and Vγ6$^+$ T cells, both skin datasets were analyzed together following the integrated analysis protocol of Seurat (Butler et al., 2018). Briefly, the top 1500 hvg of either Vγ4$^+$ or Vγ6$^+$ T cells were subjected to canonical correlation analysis (CCA) by 'RunCCA' function in Seurat. Next, CC1 – 10 were chosen for aligning into an integrated low-dimensional space (CCA.aligned). Based on CCA.aligned, we performed 'FindCluster' as above by a resolution of 0.6 and tSNE-map visualization.

QUANTIFICATION AND STATISTICAL ANALYSIS

Statistical analysis of flow cytometry data was performed using R v3.5 and GraphPad Prism software. p values $>$ 0.05 were considered as not significant. The specific test used for each experiment is indicated in the respective figure legend. For data comparison between two groups, Student's t test was utilized to determine the p value. Otherwise, we employed one-way ANOVA test with post tests indicated in the figure legends.

DATA AND SOFTWARE AVAILABILITY

The accession number for the single-cell sequencing data described in this paper is GEO: GSE123400.